

PAIReD jet: A multi-pronged resonance tagging strategy across all Lorentz boosts

Spandan Mondal* Gaetano Barone* Alexander Schmidt[§]

Abstract

We propose a new approach of jet-based event reconstruction that aims to optimally exploit correlations between the products of a hadronic multi-pronged decay across all Lorentz boost regimes. The new approach utilizes clustered small-radius jets as seeds to define unconventional jets, referred to as PAIReD jets. The constituents of these jets are subsequently used as inputs to machine learning-based algorithms to identify the flavor content of the jet. We demonstrate that this approach achieves higher efficiencies in the reconstruction of signal events containing heavy-flavor jets compared to other event reconstruction strategies at all Lorentz boost regimes. Classifiers trained on PAIReD jets also have significantly better background rejections compared to those based on traditional event reconstruction approaches using small-radius jets at low Lorentz boost regimes. The combined effect of a higher signal reconstruction efficiency and better classification performance results in a two to four times stronger rejection of light-flavor jets compared to conventional strategies at low Lorentz-boosts, and rejection rates similar to classifiers based on large-radius multi-pronged jets at high Lorentz-boost regimes.

*Brown University, Providence, USA

[§]RWTH Aachen University, Aachen, Germany

1 Introduction

Jets are ubiquitous in collider physics experiments. A jet may originate from a single quark/gluon generated in the hard scattering, or from the hadronic decay of a heavy Lorentz-boosted object, such as a W, Z, or Higgs (H) boson. In the former case, the jet is expected to have a single-pronged structure¹, while in the latter, it is expected to have a multi-pronged structure. While looking at a jet as a single object does not let us distinguish between these categories in general, investigation into jet substructures [1–3] provides additional handles to predict the nature of the particle that resulted in the jet. More recent developments use machine learning architectures to achieve unprecedented accuracies in jet identification tasks [3–6].

The choice of one or more jet reconstruction algorithms in analysis of collision data depends on several factors, such as the composition of the expected final state and the Lorentz-boosts of physics objects. For example, a search for the Higgs boson decaying to heavy-flavor (bottom or charm) quarks may be divided into two distinct reconstruction-strategy regimes [7, 8]: (i) a resolved-jet regime, when the Higgs boson has a low Lorentz boost (transverse momentum, $p_T \lesssim 200$ GeV) and the two quarks arising from the Higgs boson have a large angular separation (opening angle), giving rise to two separate small-radius, single-pronged jets, and (ii) a merged-jet or boosted regime, when the Higgs boson has a high Lorentz boost ($p_T \gtrsim 200$ GeV), and the decay products of the Higgs boson can be reconstructed with either two small-radius jets or one large-radius, multi-pronged jet, owing to a smaller angular separation. Heavy-flavor decays of the Higgs boson can then be selected using jet flavor identification algorithms. In case of single-pronged small-radius jets, jet identification usually involves identifying the flavor of the quark or gluon that initiated the jet (flavor tagging) [9]. Hence, flavor-tagging classifiers that discriminate between bottom (b), charm (c) and light-flavor (up, down, strange, gluon) jets are employed. On the other hand, for multi-pronged jets, either flavor identification or heavy object identification algorithms are employed [10]. In the discussed example, one might use a multiclassifier that discriminates between $H(H \rightarrow b\bar{b})$, $H(H \rightarrow c\bar{c})$, and light-flavor jets.

The choice of using one large-radius jet instead of two small-radius jets in the boosted regime is motivated by several factors. When a heavy object identification or jet flavor identification algorithm is used to identify a large-radius jet, it can exploit not only the information of the two (or more) subjects contained in the jet, but also the correlations that exist between the kinematics of the hadronization products of the two (or more) quarks. In addition, the large-radius jet potentially encompasses soft radiations that may lie spatially between the subjects. The presence and kinematics of these particles may provide additional handles to discriminate resonant subject pairs against non-resonant ones, as the former are expected to exhibit electrical charge and Quantum Chromodynamics (QCD) color recombination. Small-radius jets can also be used to reconstruct events in the boosted regime, but each jet must be flavor-tagged individually. This means that the flavor identification algorithm has access to the substructures of the small-radius jets individually and cannot take advantage of correlations between the constituents of the two jets, which inevitably results in loss of information. On the other hand, the large-radius jet approach is not suitable at low Lorentz-boosts of the Higgs boson as the decay products of the two quarks are expected to have a large angular separation. The event is therefore reconstructed with

¹The top quark is an exception. It decays into a bottom quark and a W boson before hadronizing, resulting in top quark jets having a multi-pronged structure.

two small-radius jets. It can be noted that the resolved regime usually caters to a large fraction of potentially interesting physics processes (e.g. nearly 95% of the signal in Ref. [8]) and hence the small-radius jet approach has the advantage of probing a large part of the signal phase space.

We refer to the choice of using either two small-radius (e.g. AK4) jets [11], or one large-radius (e.g. AK15) jet [8] per event as a choice of the event reconstruction strategy. This is different from choosing a jet tagging algorithm (e.g. ParticleNet [12], Particle Transformer [13], ParticleTransformerAK4 [14] used in the CMS experiment, GN1 [15] used in the ATLAS experiment, etc.) to identify the jet content. In this paper, we examine several reconstruction strategies and evaluate their performance relative to a fixed tagging algorithm. We propose a new event reconstruction strategy called **P**article **A**ngular-separation **I**ndependent **R**esonant **D**i-jet (PAIReD jet) tagging, with the goal of optimally exploiting the available information in pairs of small-radius jets to identify resonant decays of heavy particles irrespective of the angular separation of the two decay products. This allows modern flavor-tagging algorithms to exploit as much information as large-radius jet tagging algorithms typically have access to, without being restricted to a narrow range of the parent particle momentum.

Custom jets derived from reconstructed standard jets have been studied and utilized in experiments previously, for example, in the form of *megajets* in supersymmetry searches [16, 17] and reclustering large-radius jets by using properties of small-radius jets [18–20]. Methods to improve measurements involving dijet resonances using novel observables have also been proposed [21].

Section 2 outlines the PAIReD jet tagging strategy. Section 3 describes the simulation of several physics processes which are used to compare the performances of different event reconstruction strategies. Sections 4 and 5 describe the architecture and implementation of machine learning algorithms that are used to train classifiers to identify heavy-flavor Higgs boson decays. A mock $ZH(H \rightarrow c\bar{c})$ analysis is outlined in Sec. 6 as an example and the reconstruction efficiencies and classifier performances in the context of reconstructing $H \rightarrow c\bar{c}$ decays are compared across various event reconstruction strategies. Section 7 provides an outlook and Sec. 8 provides a summary and conclusion of the topics discussed in the paper.

2 The PAIReD jet strategy

A PAIReD jet is defined by the union of all the reconstructed particles that lie within a radius of $\Delta R = R_0$ around the centers of two clustered small-radius jets present in the event, where R_0 is the distance parameter used to cluster the small-radius jets and $\Delta R = \sqrt{\Delta\eta^2 + \Delta\phi^2}$ is the angular distance calculated in pseudorapidity–azimuth (η – ϕ) coordinates, with ϕ being in radians. Thus, for an event with n ($n \geq 2$) clustered AK4 jets², one can define $\binom{n}{2}$ PAIReD jets in the event, where $\binom{n}{2}$ denotes the number of ways one can choose 2 objects from a set of n objects.

This is practically implemented by calculating distances $(\Delta R_{j_1}, \Delta R_{j_2})$ of each reconstructed particle in the event from the centers of the two small-radius jets, j_1 and j_2 ; the particles satisfying

²For the sake of simplicity, we use “AK4 jets” and “small-radius jets” interchangeably henceforth. The PAIReD jet strategy can nevertheless be extended to jets clustered with any clustering algorithm, with distance parameters suitable for single-pronged decays.

$\min(\Delta R_{j_1}, \Delta R_{j_2}) < R_0$ constitute the list of constituents of the PAIReD jet. As some tagging algorithms may require ordered sets of particles, a reordering of the list of constituents, e.g. in descending order of particle p_T , may be necessary. It can be noted that this is distinct from simply concatenating the lists of constituents clustered within the two AK4 jets. As shown in Table 1 and discussed in the following paragraphs, this definition allows the PAIReD jet to reconstruct a larger fraction of the particles arising from the Higgs boson decay. On the other hand, the advantages that commonly used sequential clustering algorithms provide, such as infrared and collinear (IRC) safety [22], are not realized in this approach. A more detailed discussion about the effect of using sequential clustering algorithms has been presented in Appendix F. An alternative variant of the PAIReD approach, called the PAIReDClustered approach, that uses only the particles clustered in the two constituent AK4 jets, is discussed in Appendix F.1. The PAIReDClustered approach achieves a marginally lower performance than the baseline PAIReD approach.

Since a PAIReD jet is composed of the hadronization products of both quarks, a tagging algorithm employed to identify the hadronic decay of a heavy particle has access to correlations between any pair of particles arising from the hadronization, even if two particles are reconstructed in two different AK4 jets. Furthermore, the fact that two jets arising from the same hadronic decay inherently possess distinct properties, such as charge and color, is preserved when analyzing the entire PAIReD jet collectively; this information is lost when each AK4 jet is processed separately. However, unlike large-radius jets, the PAIReD jet still lacks information of the reconstructed particles that lie spatially between the two AK4 jets. This leads to the introduction of the second variant of the PAIReD jet strategy, which we refer to as the PAIReDEllipse strategy.

The PAIReDEllipse strategy defines a non-conventional jet using two clustered AK4 jets as “seeds”. The area of the PAIReDEllipse jet is defined by an elliptical region in the η - ϕ plane. The ellipse is defined such that the centers of the two seed AK4 jets lie on the major axis of the ellipse. The length b of the minor axis of the ellipse is fixed to 3 units in the η - ϕ plane, motivated by the largest jet radius ($\Delta R = 1.5$) used in recent physics analyses [8]. With the distance between the centers of the two AK4 jets denoted by ΔR_{jj} , the length of the major axis is defined as

$$a = \max(3, \Delta R_{jj} + 2)$$

units in the η - ϕ plane, so that the ellipse includes particles lying up to 1 unit away from the centers of each small-radius jet in the direction away from the center of the ellipse. As shown in Fig. 1 and discussed in the following paragraphs, this choice covers a large fraction of particles generated from the decay of a Higgs boson. We have tested that increasing these numbers does not significantly alter the final performance metrics of the PAIReDEllipse strategy.

All the particles reconstructed within the perimeter of the ellipse thus defined are considered constituents of the PAIReDEllipse jet. Thus, for a pair of AK4 jets, one can uniquely define one PAIReDEllipse jet. It can be noted that the definition of the PAIReDEllipse jet does not involve any sequential clustering algorithm, except for the ones necessary to define the centers of the seed AK4 jets, similar to the PAIReD jet scenario.

In presence of additional jets arising from initial- and final-state radiations, standard resolved-jet approaches typically involve sorting all AK4 jets in the event by certain predetermined parameters (p_T , b/c tagger score) to select the pair of jets that are most likely to arise from the decay of a heavy particle. Analogously in the PAIReD(Ellipse) jet strategy, the PAIReD(Ellipse) jet with the highest “bb/cc-jet” score can be treated as the decay of interest.

| ΔR_{cc} | Efficiency of clustering particles from Higgs boson decay (in %) | | | | |
|-----------------|--|------|------|--------|----------------|
| | AK4 | AK8 | AK15 | PAIReD | PAIReD-Ellipse |
| 1.00 ± 0.05 | 51.7 | 35.8 | 54.9 | 88.4 | 98.7 |
| 2.00 ± 0.05 | 45.3 | 21.1 | 34.2 | 71.4 | 90.9 |
| 3.00 ± 0.05 | 44.6 | 18.7 | 31.6 | 65.7 | 84.3 |
| 4.00 ± 0.05 | 34.2 | 12.9 | 26.3 | 39.5 | 62.1 |

Table 1: Mean percentage of generated particles arising from the decay of the Higgs boson in $ZH(H \rightarrow c\bar{c})$ events clustered in each reconstruction scenario at various values of ΔR_{cc} . Only generated jets with $|\eta| < 2.5$ are considered. In case of AK4, PAIReD, and PAIReDEllipse scenarios, events with at least two AK4 generated jets each with $p_T > 20$ GeV are taken into account. In case of the AK8 (AK15) strategy, events with at least 1 AK8 (AK15) jet with $p_T > 100$ (50) GeV are considered. In all cases, the percentage corresponding to the jet(s) reconstructing the highest fraction of Higgs decay products in each event is reported. In case of AK4, AK8, and AK15 approaches, the list of constituents clustered within generated jets are considered, while in case of PAIReD and PAIReDEllipse approaches, the distances of each generated particle from the center of the two constituent AK4 jets are considered.

Figure 1 demonstrates the effective areas in the η - ϕ plane covered by the different jet construction strategies, using simulated $ZH(H \rightarrow c\bar{c})$ events. The details of the simulation are presented in Sec. 3. It can be seen from the figure that the AK15 reconstruction strategy covers nearly the entire Higgs boson decay when the angular separation ΔR_{cc} between the two generated c quarks from the Higgs boson decay is ~ 2 units or smaller. At higher separations, a potential AK15 jet would be reconstructed around only one of the quarks (or two separate AK15 jets around two quarks). On the other hand, the AK4 reconstruction strategy can be implemented at all angular separation regimes. However, it can be seen from Fig. 1 that a significant fraction of the generated particles arising from the Higgs boson decays lie outside the effective combined area covered by the two AK4 jets. The PAIReD approach, which simply concatenates the list of particles lying in a 0.4 radius around the centers of two AK4 jets, would analogously fail to cover a significant fraction of the generated particles. Finally, the PAIReDEllipse approach covers a larger area and contains most of the generated particles arising from the Higgs boson decay at all angular separations.

Table 1 shows the mean percentage of generated particles arising from the decay of the Higgs boson that are clustered/contained within the jet(s) for each reconstruction scenario at different values of ΔR_{cc} . The numbers reported are obtained after pileup simulation and pileup subtraction (details in Sec. 3). As expected, the fraction of particles clustered within single AK8 and AK15 jets decrease with increasing angular separation. In all scenarios, using the PAIReD approach reconstructs a larger fraction of the Higgs boson decay than using 2 AK4 jets. This motivates the use of all particles lying within a characteristic angular distance from the AK4 jet centers over using particles clustered within the AK4 jets. Finally, the PAIReDEllipse approach reconstructs the maximum fraction of Higgs boson decay products in all scenarios.

Even though the higher area covered by the PAIReDEllipse jet strategy allows capturing the

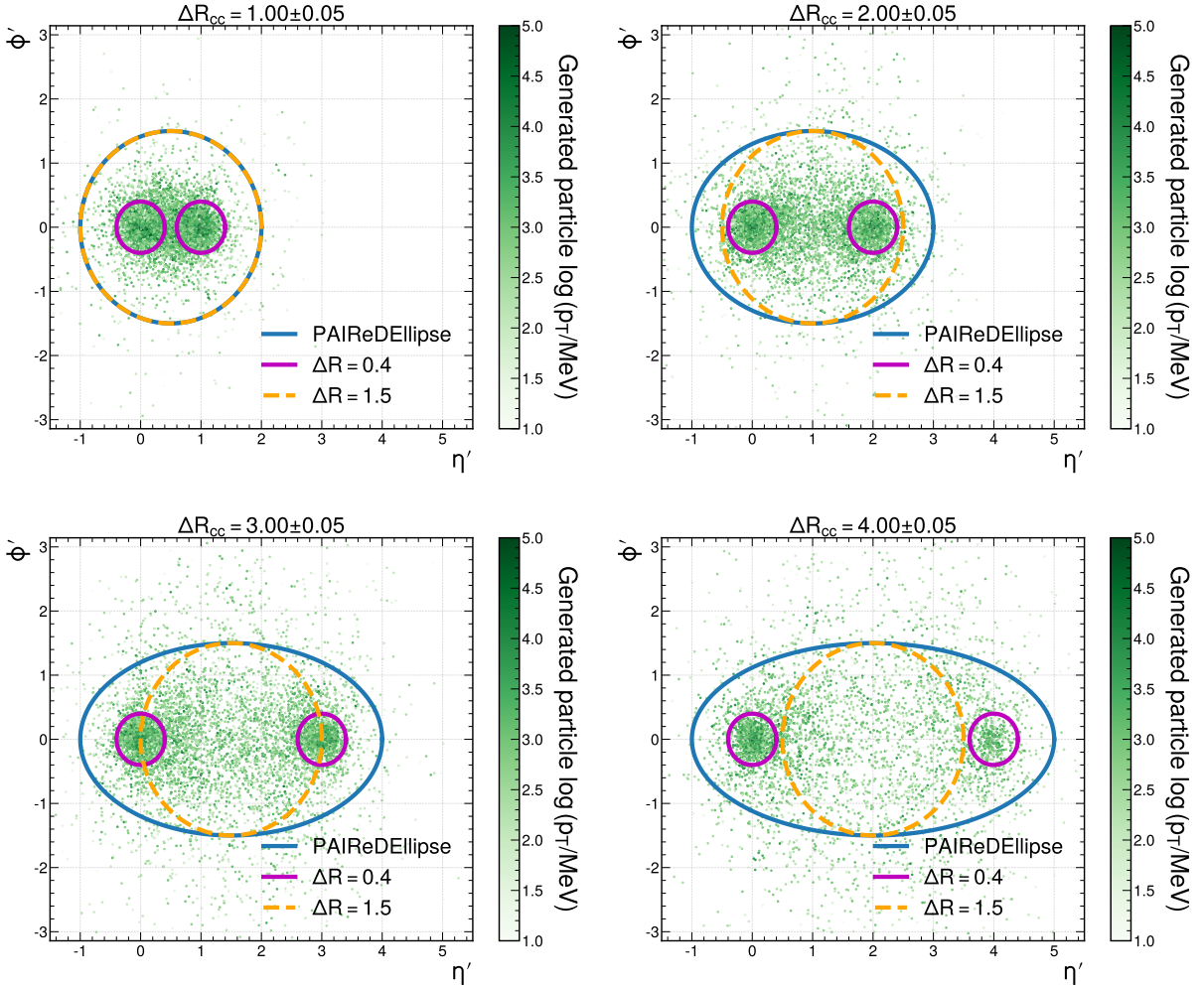


Figure 1: Simulated $ZH(H \rightarrow c\bar{c})$ events with the η - ϕ coordinate system translated and rotated in a way such that the c quark with the higher p_T is located at $(\eta', \phi') = (0, 0)$, while the second c quark lies on the η' axis ($\phi' = 0$). Each subfigure shows generated particles in 200 events, allowing particles across events to overlap. The shade of green denoting each particle is chosen according to the (logarithm of the) particle p_T , shown on the colorbar to the right of each plot. The upper-left, upper-right, lower-left, and lower-right subfigures show events with the angular separation ΔR_{cc} between the two c quarks lying in a window of 0.05 unit around 1, 2, 3, and 4, respectively. Each of the magenta circles represents the area of a potential AK4 jet that might be clustered centering one of the quarks. The two magenta circles together represent the net area covered by a jet defined using the PAIReD jet strategy. The blue ellipse represents the area of a jet defined using the PAIReDEllipse strategy. The dashed orange line represents the typical area a hypothetical AK15 jet would cover, had it been constructed at the center of the 2-quark system (see discussion in text).

entire Higgs boson decay regardless of the angular separation of the decay products, it comes at the cost of capturing additional unwanted particles, such as those arising from pileup interactions, underlying event (UE), and other unrelated hadronic activities. However, with the advent of high-level, attention-based [23] networks used for jet identification, it is expected that such spurious particles would be identified and assigned less importance while performing classification tasks downstream. Additionally, the inclusion of IRC-unsafe observables, unclustered particles, and soft radiations as inputs to the tagging algorithms potentially introduces a larger dependence of the tagger performance on the modeling of the parton shower (PS) and hadronization, modeling of the UE, and simulation-specific artifacts that do not model the collision data correctly. While a systematic study with different generators and PS models and their effects on modern ML-based tagging algorithms is beyond the direct scope of this study, a discussion about the effect of clustering algorithms and an ablated variant excluding unclustered particles are presented in Appendix F. The increased model dependency of these taggers also sheds light on the importance of calibrating the outputs of the tagger using collision data, to mitigate these dependencies as well as potential mismodelings in simulation.

In the case of PAIReD(Ellipse) jets, the momentum and other kinematic features of the jet may be calibrated in two ways. Since experiments routinely derive jet energy scale and resolution corrections for small-radius jets [24, 25] for use in a broad range of physics analyses, one may repurpose the corrected kinematics of the constituent small-radius jets to define the effective momentum and invariant mass of the PAIReD(Ellipse) jets. Thus, adding the corrected four-momenta of two constituent AK4 jets to define the effective four-momentum of the PAIReD(Ellipse) jet may be considered as the first, simple approach towards calibrating energy scales of PAIReD(Ellipse) jets. However, a more precise mass (see Appendix A) and momentum³ estimate of the initiating particle may be achieved by using mass and momentum regression techniques using all constituents of the PAIReD(Ellipse) jets as inputs. In order to calibrate the regressed (predicted) momentum, one may use event samples enriched in leptonically-decaying Z bosons recoiling against two small-radius jets (or equivalently, one PAIReD(Ellipse) jet), a standard method used for calibrating energy scales of individual small-radius jets [24, 25]. Since the momentum of a leptonic Z boson can be reconstructed with high precision, a system of Z boson recoiling against a PAIReD(Ellipse) jet lets one measure the momentum of the jet with high precision and hence derive corrections to the regressed momentum. The regressed mass may be calibrated using standard techniques to calibrate masses of large-radius jets [8]. This includes, for instance, reconstructing hadronically-decaying W bosons with PAIReD(Ellipse) jets in events enriched in semileptonic top quark-antiquark pair production ($t\bar{t}$), and comparing the mass resolution in simulation and data.

The flavor tagging efficiency of PAIReD(Ellipse) jets can similarly be compared in simulation and data using standard calibration methods used for large-radius jets. These methods involve using the kinematics of soft-muons or secondary vertices contained inside the jets to select a subset of QCD multijet events in data that mimic $b\bar{b}$ or $c\bar{c}$ jets in terms of tagger score distributions [9]. More recent methods [26, 27] make use of Boosted Decision Trees (BDTs) [28, 29] to achieve the same goal for highly performant taggers. Similar methods may be used to isolate a subset of QCD multijet events in data that mimic $b\bar{b}$ or $c\bar{c}$ PAIReD(Ellipse) jets in terms of tagger score distributions, followed by a fit to data to extract correction factors at different efficiencies. Calibration is a challenge that experiments must overcome before PAIReD(Ellipse) jets can be

³Whether regressing the momentum of PAIReD(Ellipse) jets provides a substantial advantage over using the sum of the four-momenta of two constituent AK4 jets has not been studied in this paper.

used in physics analyses. Detailed demonstration of specific calibration methods is beyond the scope of this paper.

3 Simulation

We simulate proton–proton collision events to train, validate, and compare the performance metrics across various event reconstruction strategies. We focus on the 2-lepton channel of $H \rightarrow b\bar{b}/c\bar{c}$ searches, where the Higgs boson is produced in association with a vector boson (Z/W) [8, 11, 30, 31] and the Z boson decays to a pair of electrons or muons. We refer to the $ZH(H \rightarrow b\bar{b}/c\bar{c})$ process as the signal process. The major background of these searches are $Z+jj$ events, where the Z boson decays to a pair of electrons or muons and is generated in association with two additional jets. Additionally, the semileptonic $t\bar{t}$ process forms a major background specifically in the W -associated production mode of the Higgs boson. Only $Z+jj$ and $t\bar{t}$ backgrounds have been simulated for this study.

All processes are generated with `MADGRAPH5_AMC@NLO` (MG5) [32] at leading order accuracy in QCD, with up to 3 additional partons in the event. The center of mass energy used is $\sqrt{s} = 13$ TeV. The Higgs boson decay into heavy-flavor quarks, along with parton showering and hadronization, is simulated in `PYTHIA8` [33]. The MLM prescription [34] is used to match jets from the matrix element calculations and the PS description. Finally, the detector response is simulated in `DELPHES` [35] using the default CMS configuration available in `DELPHES`.

The effect of pileup is simulated within `DELPHES` with a mean pileup value set to 50. Particles are reconstructed using the E-Flow algorithm in `DELPHES`. Jets are clustered using the AK algorithm implemented in the `FASTJET` package [36]. Distance parameters of 0.4 (AK4), 0.8 (AK8), and 1.5 (AK15) are used, and only jets with p_T greater than 20, 100, and 50 GeV, respectively, are considered. Charged hadrons coming from pileup vertices are discarded and the residual event pileup density is used along with the jet area to perform pileup subtraction on jets [35]. The true flavor of jets is defined differently for different strategies:

- **AK4:** If at least one b quark is found within the jet radius, the jet is labeled as a true b jet. If no b quark is found⁴, but at least one c quark is found, the jet is labeled c . If neither a b nor a c quark is found, the jet is labeled $udsg$ or light-flavor.
- **AK8 and AK15:** If both generated b or c quarks arising from the Higgs boson decay lie within a radius of 0.8 (1.5) units around the jet center, the AK8 (AK15) jet is labeled as a true bb or true cc jet. Otherwise, it is labeled as an ll jet.
- **PAIReD jet:** If both generated b or c quarks arising from the Higgs boson decay lie within a radius of 0.4 units around the center of either of the two constituent AK4 jets, the PAIReD jet is labeled as a true bb or cc jet. Otherwise, it is labeled as an ll jet.
- **PAIReDEllipse jet:** If both generated b or c quarks arising from the Higgs boson decay lie within the perimeter of the ellipse defined by the jet, the PAIReDEllipse jet is labeled as a true bb or cc jet. Otherwise, it is labeled as an ll jet.

⁴Labeling a jet c , only if no b quark is found, ensures that a jet with a c quark arising from a b hadron decay is labeled as a b jet rather than a c jet.

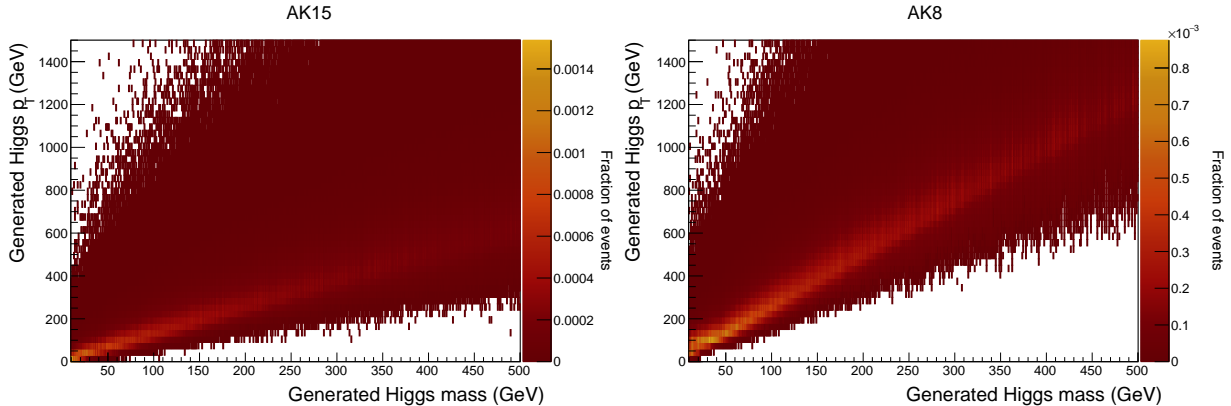


Figure 2: The fraction of AK15 (left) and AK8 (right) cc jets sampled at different values of the generated Higgs boson mass (x-axis) and p_T (y-axis) from the flat-mass $ZH(H \rightarrow c\bar{c})$ sample.

In addition to the standard Higgs boson samples discussed above, alternative samples with a variable Higgs boson mass are also generated. In these “flat-mass” samples, the mass of the Higgs boson (m_H) is set to integer values between 10 and 500 GeV with a uniform distribution, while the Higgs boson decay width is set to 4 MeV as expected from the SM [37]. These samples are used in the classifier trainings in order to achieve mass decorrelation [38–47]. The technique of using flat-mass sample to achieve decorrelation has previously been implemented in hadron collider experiments [42, 48]. Using mass decorrelated taggers ensures a fair comparison among different reconstruction strategies, since algorithms used in some strategies (e.g. AK4-based reconstruction) do not have access to the Higgs boson mass information.

An additional complexity arises in the flat-mass Higgs boson samples. The p_T spectrum of the Higgs boson is dependent on the generated mass of the Higgs boson; the fraction of events containing at least one bb/cc AK8 or AK15 jet diminishes at high masses of the Higgs boson. To mitigate this effect, an empirical Higgs boson mass-dependent selection criterion is applied⁵ on the minimum p_T of the generated Higgs boson (p_T^H) in the physics processes used to sample AK8 and AK15 jets. This criterion ranges between $p_T^H > 0$ GeV at Higgs boson mass $m_H = 10$ GeV to $p_T^H > 390$ GeV at $m_H = 500$ GeV for AK15 jets, and between $p_T^H > 0$ GeV at $m_H = 10$ GeV to $p_T^H > 900$ GeV at $m_H = 500$ GeV for AK8 jets. These selections ensure that a sufficient number of AK15 and AK8 jets are sampled throughout the Higgs boson mass range, without generating events that are unlikely to have any AK15 or AK8 jets. The distributions of AK15 and AK8 jets as functions of the generated Higgs boson mass and p_T are shown in Fig. 2 after the empirical selection criteria on p_T^H are applied.

A fraction of the simulated dataset was made available publicly for testing and development [49].

⁵The parameter `pt_min_pdg` in MG5 is used. The resulting Higgs boson p_T spectrum, however, starts at a value slightly below the applied selection criterion.

4 Flavor tagging algorithm

The algorithm used in this paper to identify the flavor of jets defined using different reconstruction strategies is the Particle Transformer (ParT) algorithm [13]. The choice of the tagging algorithm is largely independent of the choice of event reconstruction strategy and one can evaluate the performance of various reconstruction strategies relative to any one, fixed tagging algorithm.

The ParT algorithm makes use of a number of features of jet constituents as well as interactions corresponding to every pair of constituents. The network comprises of several particle and class attentions blocks. Detailed description of the network architecture can be found in Ref. [13]. As inputs, we use kinematics and trajectory displacement information of particles, but not the particle identification information. This choice is consistent with the standard methods for jet tagging used in particle physics experiments which intend to minimize potential biases in subsequent independent validation steps that exploit dedicated soft lepton information [50].

In addition to the classification tasks that have been discussed so far, the ParT algorithm is also implemented for mass regression (Appendix A) with minor changes in the architecture. For regression, the default settings were modified to use a PReLU activation function [51] and the logarithm of the hyperbolic cosine ($\log \cosh$) [52] as the loss function. In addition, a gradient clipping feature [53] was implemented to prevent gradients from becoming too large owing to the output node containing mass values of $\mathcal{O}(100)$ in units of GeV.

5 Neural network training

Several networks corresponding to the various reconstruction strategies are trained using the weaver framework [54] based on PyTorch [55], implementing the ParT architecture [13] with minor modifications as described in Sec. 4. Jets are classified into three classes, namely bb, cc, and ll (b, c, and udsg for AK4 jets). The bb (cc) jets used in the trainings are sampled from the flat-mass $ZH(H \rightarrow b\bar{b})$ ($ZH(H \rightarrow c\bar{c})$) processes. The ll jets are sampled from $ZH(H \rightarrow b\bar{b})$, $ZH(H \rightarrow c\bar{c})$, and $Z+jj$ processes. Wrong combinations of jets, such as multi-pronged jets containing only one b/c parton in the ZH processes, are also labeled ll (cf. Sec. 3). The number of ll jets sampled from each of $ZH(H \rightarrow b\bar{b})$, $ZH(H \rightarrow c\bar{c})$, and $Z+jj$ processes ranges between 25–30 million. In case of AK4 jet trainings, all jets labeled b, c, and udsg are used regardless of the physics process they were sampled from.

Jets are assigned weights during the training such that each class contains an equal number of jets. In case of AK8, AK15, PAIReD, and PAIReDEllipse trainings, the jets are weighted such that a mass metric has the same distribution for all labels, using the mass distribution of the ll jets as the reference. For the purpose of defining a uniform mass metric, mass regression techniques, discussed in Appendix A, are used. Only jets with regressed masses (m_{reg}) of 50–400 GeV are used to train the classifier, in order to avoid any biases in the prediction of m_{reg} for jets lying at the extreme edges of the range ($m_{\text{reg}} \in [10, 50] \cup (400, 500]$ GeV). In case of AK4 jets, the jets are weighted such that the p_T and η of the jets in the b and c classes have the same distributions as those in the reference udsg class.

About a tenth of the jets are used as an independent *validation dataset* to check for overtraining. The initial learning rate (LR), batch size, and number of epochs were adjusted to ensure optimal convergence and balance between model performance and training efficiency. Finally, the Ranger optimizer [56], along with a uniform configuration of batch size 2048 and initial LR of 5×10^{-3} , was chosen across all trainings, and each training was run for 80 epochs. The model from the epoch achieving highest classification accuracy on the validation dataset is selected as the final classifier model. The trainings are then evaluated on an independent *test dataset* comprising jets from $ZH(H \rightarrow b\bar{b})$ and $ZH(H \rightarrow c\bar{c})$ processes with $m_H = 125$ GeV, and an independent Z+jj sample. The performance comparison of the various classifiers corresponding to different reconstruction strategies is presented in Sec. 6.3.

6 Performance evaluation on $H \rightarrow c\bar{c}$ events

The various event reconstruction strategies outlined in this paper can be compared and contrasted using $H \rightarrow c\bar{c}$ events. In this paper, we demonstrate a mock $ZH(H \rightarrow c\bar{c})$ analysis as an example. The analysis strategies corresponding to the various reconstruction strategies are outlined in Sec. 6.2. In all cases, we ignore the reconstruction of the leptonic Z decay and focus on reconstructing the hadronic Higgs boson decay. Another example using $Z \rightarrow c\bar{c}$ events is presented in Appendix D. Only the Z+jj background with a leptonically-decaying Z boson is studied in this section. Since only the hadronic part is considered for the analysis, it is expected that the results would be similar when discriminating signal events from W+jj and Z+jj (Z decaying into neutrinos) in other channels, and hence they are not studied separately. However, since the $t\bar{t}$ background is a major background in search for the W-associated Higgs production and has a signature distinct from Z+jj events, it is studied in Appendix E, along with an extended PAIReD(Ellipse) jet tagger retrained with additional $t\bar{t}$ classes.

6.1 Performance metrics

The performances of jet flavor taggers are usually quantified using metrics such as accuracy, area under the ROC curve (AUC), background rejection at a given signal efficiency, etc. While these metrics convey useful information when evaluating the performance of different algorithms on the same type of reconstructed jets (e.g. public benchmark jet datasets [57–60]) they are not very interpretable when comparing across various event reconstruction strategies and across various Lorentz-boost regimes.

We define end-to-end selection efficiency as the fraction of simulated events that are selected and correctly reconstructed after all selection criteria and classifier score requirements are applied. This includes the requirement that a certain number of jets be reconstructed per event, as well as any requirements that are applied to the jet tagger scores to achieve a target signal efficiency. This quantity is, therefore, dependent on the reconstruction strategy being used, as well as the tagging performance achievable using that strategy. Events that cannot be reconstructed using a given reconstruction strategy, and events that are incorrectly reconstructed (e.g. wrong choice/selection of jets) contribute to a decline in the end-to-end efficiency metric. This is in contrast to the standard metrics that are used to evaluate jet tagging algorithm performances—standard metrics

focus on the background rejection for a specific type of jets, disregarding the fraction of events that contain such jets and the fraction of events where the correct jet(s) is (are) chosen. This makes the end-to-end efficiency a suitable metric to compare between event reconstruction strategies and across Lorentz-boost regimes.

The end-to-end selection efficiency can be defined for both signal and background events. They can be interpreted as the end-to-end true positive and false positive rates, respectively. A more natural metric for background events is the background rejection, which can be defined as the inverse of the background selection efficiency. Thus, one can define an end-to-end background rejection rate at a given end-to-end signal selection efficiency. Additionally, a rough estimation of the differential signal sensitivity as a function of the Higgs boson p_T is shown in Appendix B.

6.2 Event selection strategies

6.2.1 Analysis using AK4 jets

We follow the strategy adopted by the CMS $H \rightarrow c\bar{c}$ search [8] in the resolved-jet regime. Only events with at least 2 well-reconstructed AK4 jets with $p_T > 20$ GeV lying within $|\eta| < 2.5$ are selected. In each event, jets are sorted by the so-called CvsL score, which is defined as

$$\text{CvsL} = \frac{P(c)}{P(c) + P(\text{udsg})}, \quad (1)$$

where $P(c)$ and $P(\text{udsg})$ are the tagger scores obtained at the c and udsg output nodes of the classifier prediction, respectively. We verified that using $P(c)$ instead of CvsL to sort the jets did not change the results significantly. The two jets with the highest CvsL values in each event are used to reconstruct the Higgs boson candidate. The invariant mass m_{jj} of the Higgs boson candidate is required to lie within the range 50–200 GeV. The same procedure is repeated for the background sample.

Only signal events where the correct pair of AK4 jets is chosen are counted towards the “pass” events in the signal selection efficiency calculation. To obtain the end-to-end background rejection rate at a fixed (say, ϵ) end-to-end signal selection efficiency (in line with the strategy outlined in Sec. 6.1), the $P(c)$ score of the subleading jet in signal events for which exactly ϵ fraction of the signal events pass all the selection criteria is first determined. Next, the same requirement on the $P(c)$ score is applied on the subleading jet of the background events. The fraction of background events thus selected gives the end-to-end background mistag rate at an end-to-end signal efficiency of ϵ . The inverse of this quantity gives the end-to-end background rejection rate.

6.2.2 Analyses using AK8 and AK15 jets

Events with at least one AK15 (AK8) jet with $p_T > 50$ (100) GeV and $m_{\text{reg}} \in (50, 400)$ GeV, lying within the tracker acceptance ($|\eta| < 2.5$) are selected. The preselection on m_{reg} is necessary since the classifiers are trained only in a limited m_{reg} range. In each event, the jet with the highest $P(\text{cc})$ score obtained from the classifier prediction is considered as the Higgs boson candidate.

As before, only signal events where the selected jet contains both c quarks from the Higgs boson decay are counted towards the “pass” events in the signal selection efficiency calculation. Finally, an additional requirement of $m_{\text{reg}} \in (50, 200)$ GeV is applied for the selected jet.

As before, a requirement on the $P(cc)$ score for which a certain fraction of the signal events pass the selection criteria is applied to the selected jet of the background events to calculate the end-to-end background rejection rate.

6.2.3 Analyses using PAIReD and PAIReDEllipse jets

The analyses using PAIReD and PAIReDEllipse jets follow the same strategy as the ones with AK8 and AK15 jet. No minimum p_T requirement is applied for the jets, but the AK4 jets from which the PAIReD(Ellipse) jets are defined are required to have $p_T > 20$ GeV each. Events with at least one PAIReD(Ellipse) jet with $m_{\text{reg}} \in (50, 400)$ GeV lying within the tracker acceptance ($|\eta| < 2.5$) are preselected. In each event, the jet with the highest $P(cc)$ score obtained from the classifier prediction is considered as the Higgs boson candidate. Finally, a more stringent requirement of $m_{\text{reg}} \in (50, 200)$ GeV is applied for the selected jet.

Similarly as before, the same requirement on the $P(cc)$ score is applied to the selected jet of the background events and the end-to-end background rejection rate is calculated.

6.2.4 Summary

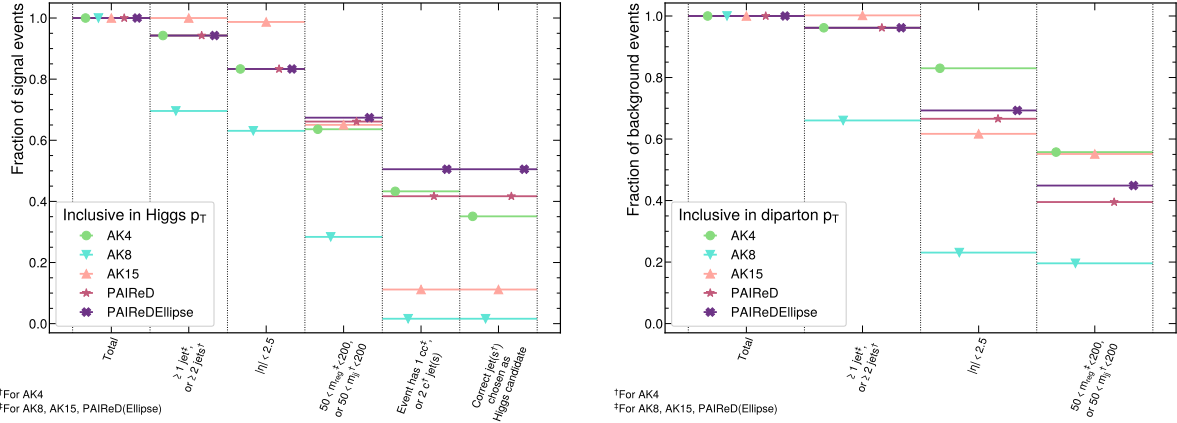
The hadronic part of the $ZH(H \rightarrow c\bar{c})$ final state is reconstructed with 5 different approaches. The fraction of signal and background events obtained after progressively applying each selection criterion is shown in so-called cutflow plots at different p_T ranges of the Higgs boson (or diparton system) in Fig. 3. These cutflow plots exclude the final requirement on the classifier scores applied to obtain a fixed signal efficiency.

6.3 Performance comparisons

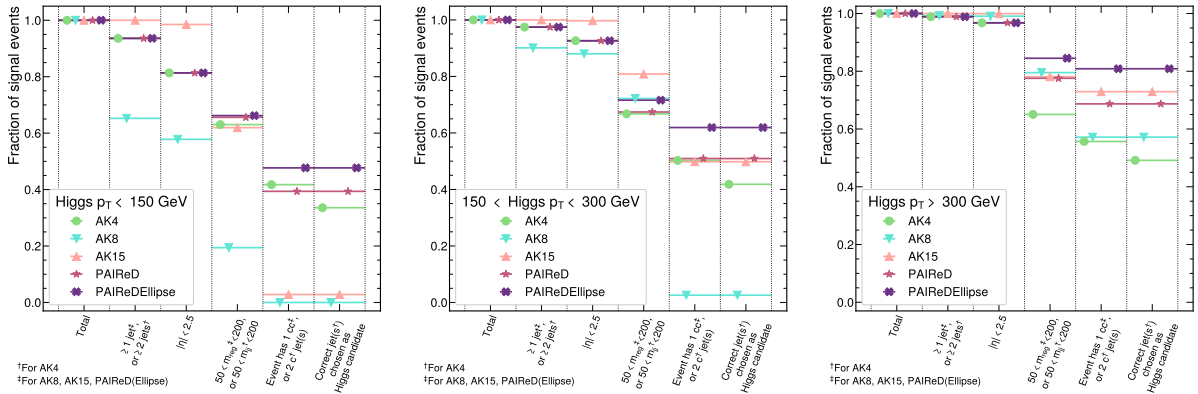
The end-to-end selection efficiency metric can be factorized into two components: (a) the reconstruction efficiency, and (b) the classifier performance. The combined effect of the signal reconstruction efficiency and the classifier performance determines the final analysis sensitivity. For instance, a poorer classifier performance can offset any gains achieved from having a high signal reconstruction efficiency. The two efficiencies are investigated separately to study how each component contributes to the final gains.

6.3.1 Signal reconstruction efficiency

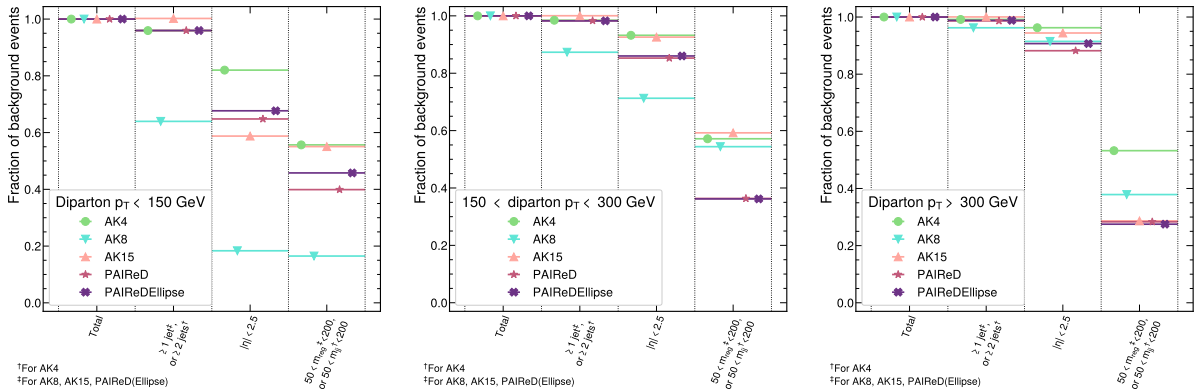
The signal reconstruction efficiency can be defined as the ratio of the maximum number of signal events that can be reconstructed using a given strategy, to the total number of events generated.



(a) Signal (left) and background (right) events, inclusively in Higgs/diparton p_T .



(b) Signal events at various ranges of the Higgs boson p_T .



(c) Background events at various ranges of the diparton system p_T .

Figure 3: Plots showing fraction of signal or background events obtained after each selection criterion is progressively applied. The last two selections in Fig. 3a (left) and Fig. 3b involve using generator-level flavor information in signal samples to investigate how many correctly reconstructed events pass the selection criteria. Selections are, in general, different for small-radius (AK4) and large-radius (AK8, AK15, PAIReD, PAIReDEllipse) jets, and are marked using † and ‡, respectively. The masses are in units of GeV.

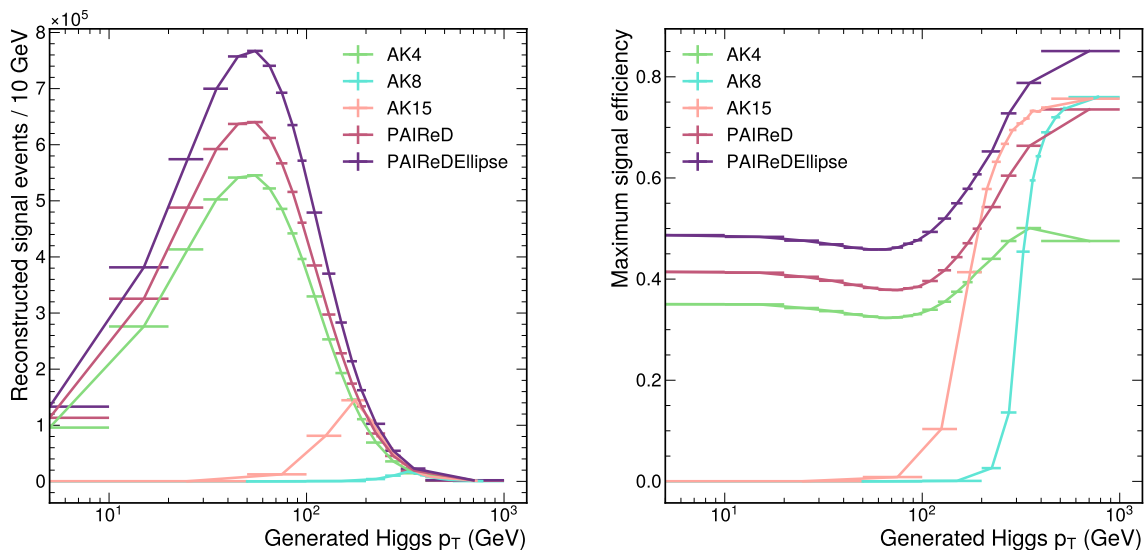


Figure 4: The number of reconstructed $ZH(H \rightarrow c\bar{c})$ signal events out of the 10M signal events generated (left) and the signal reconstruction efficiency (right) as functions of the generated Higgs boson p_T , for various reconstruction strategies.

This involves calculating the signal efficiency in each of the analyses without applying the requirement on the classifier output score (cf. Sec. 6). This metric can also be considered as the maximum signal efficiency that can be achieved using a particular reconstruction strategy.

The signal reconstruction efficiency is evaluated using the $ZH(H \rightarrow c\bar{c})$ process at various ranges of the generated Higgs boson p_T . A comparison of the yield of reconstructed signal events and the signal reconstruction efficiency across various reconstruction strategies is presented in Fig. 4. The PAIReDEllipse strategy improves the signal reconstruction efficiency by about 40–50% compared to AK4-based event reconstruction at low Lorentz-boosts ($\lesssim 200$ GeV) of the Higgs boson. The efficiency of the PAIReDEllipse strategy is slightly higher (~ 2 –14%) compared to that of the AK15-based strategy at higher boosts. The PAIReD strategy has efficiencies intermediate to that of the AK4 and PAIReDEllipse approaches, as expected. The AK4, PAIReD, and PAIReDEllipse approaches reconstruct a significantly larger number of signal events compared to the AK8 and AK15-based approaches. The gain comes mainly from the low Lorentz-boost regime.

6.3.2 Classifier performance

The ability of classifiers to distinguish between signal and background jets is also expected to vary across different reconstruction strategies. Classifiers trained using AK4 jets, for instance, evidently have access to less information than classifiers trained with AK15 jets and hence are expected to have lower background rejection rates.

The classifier performances are evaluated by calculating the AUC using all the signal and background events that pass the selection criteria (except the requirement on the classifier output

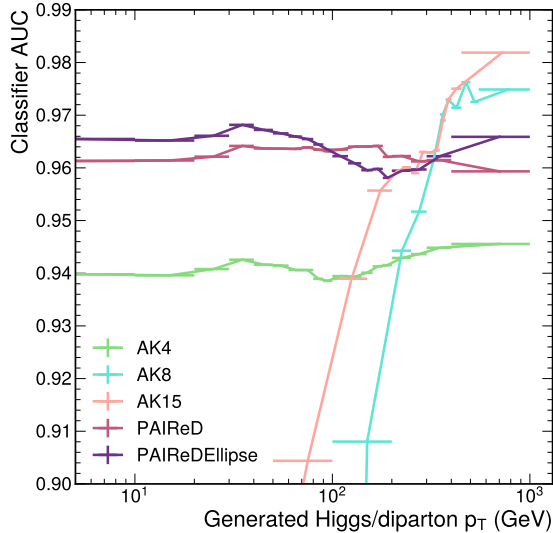


Figure 5: The area under the ROC curves (AUC) obtained when classifiers corresponding to various reconstruction strategies are evaluated on the signal and background events passing the respective selection criteria, plotted as a function of the Higgs boson p_T (for signal events) or the diparton p_T (for background events).

score). Furthermore, a proxy Higgs boson p_T needs to be defined for the background events in order to evaluate the AUC performances at different Lorentz-boosts of the generated Higgs boson. For this purpose, a diparton p_T is defined by adding the four-vectors of the two MG5-level partons produced in association with a Z boson in the background Z+ jj events. The diparton p_T is used as the proxy for Higgs boson p_T in the background events. The motivation behind this choice is that the fake Higgs boson candidate defined in the background events passing the selection criteria is most likely reconstructed from the hadronization products of the two associated MG5-level partons in the Z+ jj events. Therefore, the generator-level diparton system in background events is a suitable proxy for the generator-level Higgs boson in signal events.

The AUCs of the classifiers corresponding to the various reconstruction strategies are compared in Fig. 5. The classifiers corresponding to the PAIReD and PAIReDEllipse strategies have comparable performances and outperform those corresponding to other strategies in the low boost regimes. In the high boost regimes, the AK15- and AK8-based classifiers outperform other classifiers. The improvement compared to PAIReD and PAIReDEllipse approaches at high boosts can be attributed to the fact that AK8 and AK15 jets are constructed using IRC-safe sequential clustering algorithms and are less sensitive to presence of pileup particles. This is discussed in more detail in Appendix F.

6.3.3 End-to-end efficiencies

The end-to-end background rejection rates at a given target end-to-end signal efficiency for different reconstruction strategies are discussed in this subsection. Figure 4 (right) shows the maximum

signal efficiency achievable at different boosts of the generated Higgs boson. As AK4 jets achieve a maximum signal efficiency of around ~ 0.37 at low Lorentz-boosts, requiring a target signal efficiency above ~ 0.37 is expected to yield no sensitivity with the AK4-based reconstruction approach at low Lorentz-boosts. Nevertheless, end-to-end signal efficiencies of 0.4, 0.3, 0.2, and 0.1 are explored and the corresponding background rejection rates as a function of the Higgs/diparton p_T are shown in Fig. 6. The end-to-end signal efficiencies and background rejections are calculated per bin, i.e. exclusively in the Higgs/diparton p_T range covered by each bin.

At low Lorentz-boosts of the Higgs boson, the PAIReDEllipse strategy performs the best with around 2.5-4 times higher background rejection compared to the AK4 strategy. The PAIReD strategy has a performance intermediate to that of AK4 and PAIReDEllipse strategies, with around 2-3 times improvement compared to AK4-based reconstruction. Both AK4 and PAIReD strategies fail to achieve signal efficiencies of 0.4 at Higgs boson boosts of ~ 25 – 150 GeV (cf. Fig. 4 (right)) resulting in a dip in the observed background rejection at a signal efficiency of 0.40 (Fig. 6, upper-left); this makes PAIReDEllipse the only strategy to achieve a non-zero background rejection at 0.40 signal efficiency in this boost regime. At higher boosts, the PAIReDEllipse and AK15 approaches have similar performances. The AK8 approach has comparable performances at low signal efficiencies, but performs slightly worse than PAIReDEllipse and AK15 at higher signal efficiency requirements.

6.3.4 Event-level classification

Going beyond using only jet tagger scores for signal vs. background event classification, analyses generally make use of additional event-level observables to improve signal-background separation. Jet kinematics, Higgs boson candidate mass and p_T , lepton kinematics, and Z boson candidate kinematics, e.g., may provide additional information to differentiate $ZH(H \rightarrow c\bar{c})$ events from $Z+jj$ background. Similar to Refs. [7, 8], event-level BDTs are trained to distinguish signal events from background events. The BDTs use the jet tagger scores along with various kinematic quantities associated with events as inputs. Observables related to the leptons and Z boson candidate are not used as inputs to the BDT for simplicity. Five different BDTs, corresponding to the five different event reconstruction approaches, are trained using different sets of observables relevant to the corresponding event reconstruction approach. Table 2 shows the sets of event-level observables used as inputs to the BDTs. It can be noted that unlike performance metrics discussed until Sec. 6.3.3, the event-level BDT discussed here is not agnostic to the mass of the Higgs boson candidate by design.

The BDTs are implemented as Gradient Boosting Machines [61] using the XGBOOST library [62] in Python [63], while tools in the SCIKIT-LEARN package [64] are used for data handling. Half (~ 5 M $ZH(H \rightarrow c\bar{c})$ with $m_H = 125$ GeV and ~ 5 M $Z+jj$ events) of the generated dataset (referred to as *test dataset* in Sec. 5) is considered for training the BDTs. Of these events, only those passing the event selections for a given event reconstruction approach are used in training the corresponding BDT. Each model is trained to minimize the fraction of misclassified instances (error rate) during training.

The trained BDT models are then evaluated on the remaining half of the *test dataset*. For each event reconstruction approach, the end-to-end background event rejection rate as predicted by

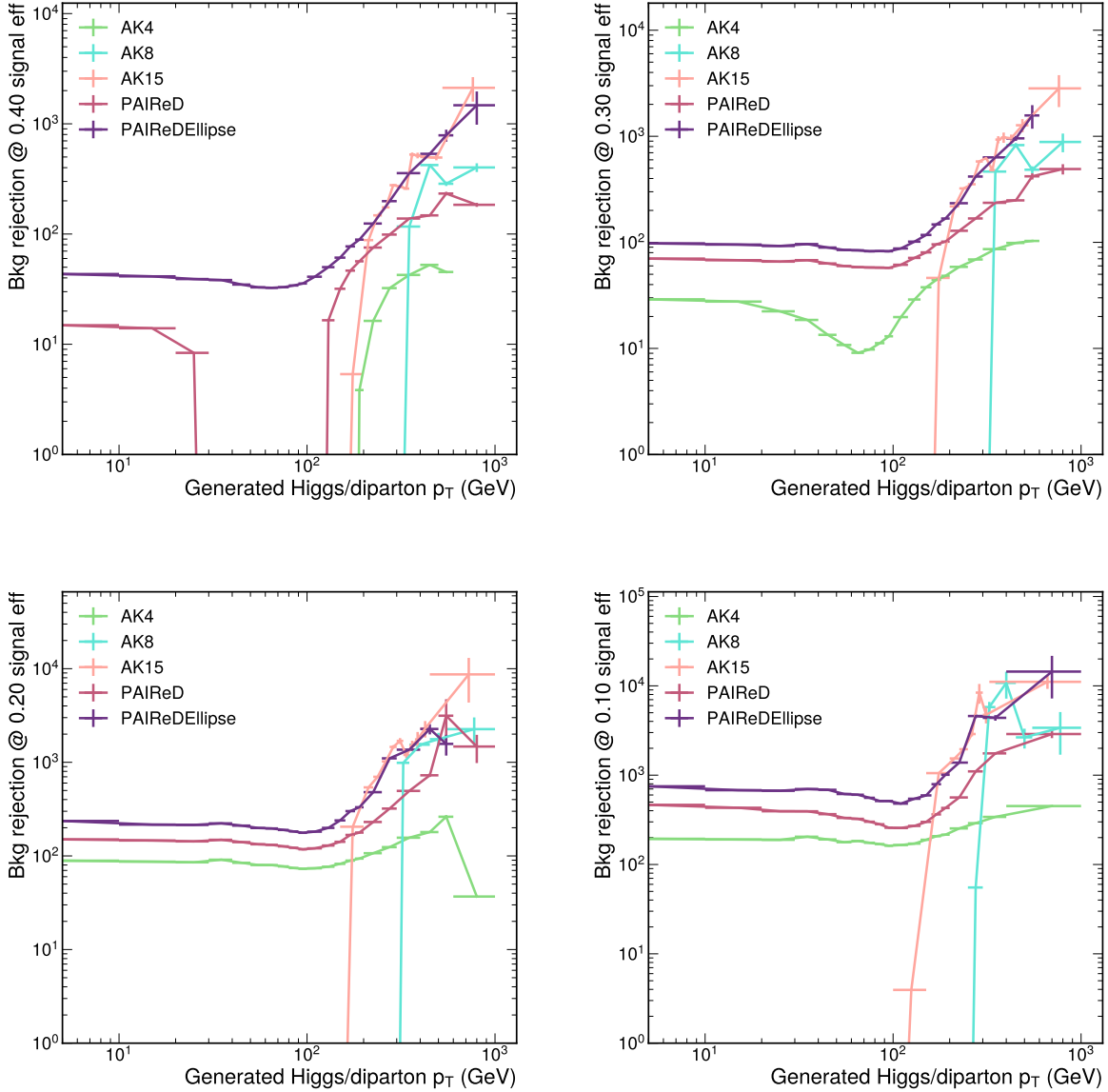


Figure 6: The end-to-end background rejection at end-to-end signal efficiencies of 0.4 (upper-left), 0.3 (upper-right), 0.2 (lower-left), and 0.1 (lower-right) as a function of the generated Higgs boson p_T (for signal) or diparton p_T (for background), plotted for various reconstruction strategies. End-to-end signal efficiencies and background rejections are calculated per bin. The background rejection is set to 0 wherever the target signal efficiency cannot be achieved. Bins with very low yield of background events are either merged with adjacent bins or are omitted.

| Observable | AK4 | AK8 | AK15 | PAIReD | PAIReD-Ellipse |
|-----------------------------------|-----|-----|------|--------|----------------|
| AK4 jet 1 kinematics | ✓ | | | ✓ | ✓ |
| AK4 jet 1 CvsL score | ✓ | | | | |
| AK4 jet 1 CvsB score | ✓ | | | | |
| AK4 jet 2 kinematics | ✓ | | | ✓ | ✓ |
| AK4 jet 2 CvsL score | ✓ | | | | |
| AK4 jet 2 CvsB score | ✓ | | | | |
| PAIReD/Fat jet kinematics | | ✓ | ✓ | | |
| PAIReD/Fat jet CCvsLL | | ✓ | ✓ | ✓ | ✓ |
| PAIReD/Fat jet CCvsBB | | ✓ | ✓ | ✓ | ✓ |
| Higgs candidate mass (dijet mass) | ✓ | | | | |
| Higgs candidate mass (regressed) | | ✓ | ✓ | ✓ | ✓ |
| Higgs candidate p_T | ✓ | (✓) | (✓) | | |

Table 2: List of inputs to the various event-level BDTs. Jet kinematics refer to p_T , η , ϕ , and energy of the jet. The Higgs candidate mass refers to the regressed mass in case of fat and PAIReD(Ellipse) jets and dijet invariant mass in case of AK4 jets. The Higgs candidate p_T and fat jet p_T are equivalent in case of fat jets. CvsB is defined as $CvsB = \frac{P(c)}{P(c)+P(b)}$, in the same fashion as in eq. 1. Similarly CCvsLL and CCvsBB are defined as $CCvsLL = \frac{P(cc)}{P(cc)+P(ll)}$ and $CCvsBB = \frac{P(cc)}{P(cc)+P(bb)}$.

the corresponding BDT is plotted as a function of the end-to-end signal efficiency. Figure 7 shows the performance of these event-level BDTs at various ranges of the Higgs p_T . Inclusively in p_T , the PAIReDEllipse approach achieves 2–2.5 times better background rejection compared to the AK4 approach, depending on the target signal efficiency, while the PAIReD approach has an intermediate performance. The AK15 and AK8 approaches do not play a significant role in low p_T 's, but surpass the AK4-based approach at high p_T 's. At all p_T ranges, the BDT corresponding to the PAIReDEllipse approach exhibits the best classification performance. The performance of the BDTs as a function of the Higgs p_T and at different jet multiplicities, along with some discussions, is presented in Appendix C.

An additional variant of the AK4-based BDT was trained using the kinematic information of a third jet in the event (whenever reconstructed), and a second Higgs mass input reconstructed from the four-vectors of three AK4 jets. This was done with the motivation to capture a possible third jet arising from final state radiations. However, this BDT performed only marginally better ($\sim 0.03\%$ improvement in the accuracy metric) compared to the nominal AK4-based BDT and hence was not used.

7 Outlook

The PAIReD(Ellipse) approaches potentially leverage information across a larger volume of the detector, especially at low boosts, while the related observables are still calibratable using modified versions of the standard jet calibration techniques used in hadron collider experiments. The approach can be generalized to multi-pronged decays as well, as long as suitable event samples can be identified in collision data for calibration. A three-pronged tagger, for example, may be calibrated using hadronically-decaying top quark events.

Furthermore, more complex final states, like 4b, 6b, 8b, and so on, can potentially be factorized into two or more two-pronged PAIReD(Ellipse) jets for reconstruction. The classifier output scores are expected to be higher for the correct pairs of b quark resonances, which can help identify the correct combinations of small-radius jets potentially in conjunction with jet assignment algorithms [65–67]. Tagger calibration for such complex final states can be achieved by evaluating correction factors for simulated events as a function of the efficiency correction factors of all PAIReD(Ellipse) jets reconstructed in the event. The strategy may also be used to discriminate events containing resonant heavy-flavor decays ($H \rightarrow b\bar{b}$, for example) from those containing non-resonant decays (b and \bar{b} from $t\bar{t}$ decay) at low boosts, without using the invariant mass information. These extended use cases, however, require additional studies and may be studied systematically for different high-multiplicity final states in the future.

The method can also be suitably modified to identify, for example, charged Higgs boson decays into $c\bar{s}$, by introducing additional cs flavor nodes in the outputs. Such a classifier can be calibrated using hadronically-decaying W bosons from $t\bar{t}$ events, for instance. Thus, the PAIReD and PAIReDEllipse approaches may be extended to several kinds of physics analyses.

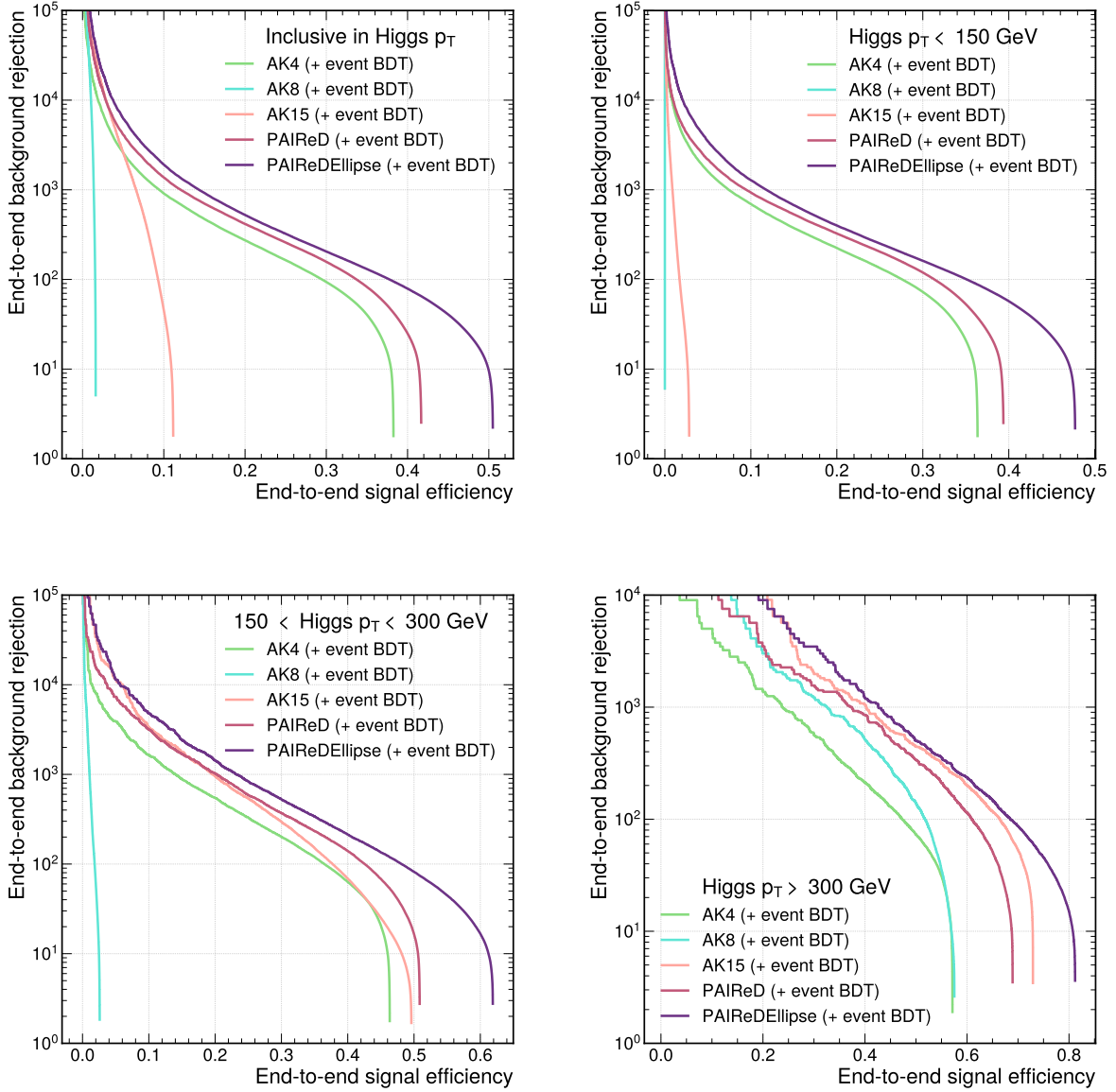


Figure 7: The end-to-end background event rejection rate as a function of the end-to-end signal efficiency inclusively in Higgs boson (or diparton) p_T (upper-left), at low ($p_T < 150$ GeV) p_T ranges (upper-right), at medium ($150 < p_T < 300$ GeV) p_T ranges (lower-left), and at high ($p_T > 300$ GeV) p_T ranges (lower-right), as predicted by the event-level BDT. The highest value along the x-axis reached by each curve represents the maximum signal reconstruction efficiency achievable using the respective event reconstruction strategy (cf. Sec. 6.3.1), while the lowest value along the y-axis for each curve represents the trivial background rejection achieved from reconstructing the event with reconstructed physics objects satisfying quality criteria (i.e. without any selection criterion on the BDT output).

8 Conclusion

We propose a new method to reconstruct events containing hadronically-decaying heavy particles. The two variants of the method, namely PAIReD and PAIReDEllipse jet based reconstruction, define unconventional jets using clustered small-radius jets as seeds. The former is limited to the area defined by the small-radius jets, whereas the latter defines an elliptical area in the η - ϕ plane based on the centers of the small-radius jets and considers all reconstructed particles lying in this area as jet constituents.

We have demonstrated this method in the context of di-pronged resonances, where the PAIReD-(Ellipse) jets are constructed from exactly two AK4 jets. We have examined two rare physics processes, namely Higgs bosons decaying to a bottom or charm quark-antiquark pair, where the Higgs boson is produced in association with a Z boson ($ZH(H \rightarrow b\bar{b}/c\bar{c})$). We have used the ParticleTransformer jet tagging algorithm for regression and classification tasks. We have trained mass-decorrelated multi-classifiers to discriminate $b\bar{b}$, $c\bar{c}$, and light-flavor jets (b, c and udsg, for AK4 jets).

The PAIReDEllipse strategy has the highest signal reconstruction efficiency at all Lorentz-boosts of the Higgs boson. The AK4, PAIReD, and PAIReDEllipse approaches reconstruct significantly more signal events than AK15 and AK8 approaches, while the AK15 and AK8 surpass the AK4-based approach in terms of signal efficiency at high boosts. In terms of classifier performance, the PAIReDEllipse and PAIReD perform better than AK4 at all boosts, while the AK15 and AK8 classifiers surpass all others at high boosts. The combined effect results in the PAIReDEllipse approach having a background rejection about 2.5–4 times higher than the AK4-based approach at low boosts, while the PAIReD approach performs about 2–3 times better than the AK4-based approach. At higher boosts, the PAIReDEllipse approach has a performance at par with the AK15-based approach.

The previous state-of-the-art analysis techniques involve using AK4-based jet reconstruction at low Higgs boson boosts ($p_T^H \lesssim 300$ GeV) and using AK15-based reconstruction at high boosts. Our proposed PAIReDEllipse tagger improves the background rejection at low boosts by up to 4 times compared to AK4-based taggers, while maintaining the same performance as AK15-based taggers at high boosts. The main gain in performance at low boosts comes from the ability of PAIReD(Ellipse)-based classifiers to exploit correlations between the hadronization products of the two quarks—a feat that was so far achieved only at high boosts using the substructure information of large-radius jets. The new method is expected to significantly improve the sensitivities of physics searches in the low-boost regime and enable searches that were previously considered inaccessible at low boosts.

Acknowledgements

We are grateful to the authors of Ref. [13], H. Qu, C. Li, and S. Qian for many helpful discussions. We are also grateful to them for publishing and sharing codes which we adapted for this work. We would also like to thank U. Heintz and J. Luo for many fruitful discussions. This research was supported by the Deutsche Forschungsgemeinschaft (DFG) under grant 400140256 - GRK 2497:

The physics of the heaviest particles at the LHC, and the U.S. Department of Energy, Office of Science, Office of Basic Energy Sciences Energy Frontier Research Centers program under Award Number DE-SC0010010. Part of this research was conducted using computational resources and services at the Center for Computation and Visualization, Brown University.

References

- [1] J. Thaler and K. Van Tilburg, “Identifying Boosted Objects with N-subjettiness”, *JHEP* **03** (2011) 015, doi:10.1007/JHEP03(2011)015, arXiv:1011.2268.
- [2] D. Adams et al., “Towards an Understanding of the Correlations in Jet Substructure”, *Eur. Phys. J. C* **75** (2015) 409, doi:10.1140/epjc/s10052-015-3587-2, arXiv:1504.00679.
- [3] R. Kogler et al., “Jet Substructure at the Large Hadron Collider: Experimental Review”, *Rev. Mod. Phys.* **91** (2019) 045003, doi:10.1103/RevModPhys.91.045003, arXiv:1803.06991.
- [4] D. Guest et al., “Jet Flavor Classification in High-Energy Physics with Deep Neural Networks”, *Phys. Rev. D* **94** (2016) 112002, doi:10.1103/PhysRevD.94.112002, arXiv:1607.08633.
- [5] D. Guest, K. Cranmer, and D. Whiteson, “Deep Learning and its Application to LHC Physics”, *Ann. Rev. Nucl. Part. Sci.* **68** (2018) 161–181, doi:10.1146/annurev-nucl-101917-021019, arXiv:1806.11484.
- [6] A. J. Larkoski, I. Moulton, and B. Nachman, “Jet Substructure at the Large Hadron Collider: A Review of Recent Advances in Theory and Machine Learning”, *Phys. Rept.* **841** (2020) 1–63, doi:10.1016/j.physrep.2019.11.001, arXiv:1709.04464.
- [7] CMS Collaboration, “A search for the standard model Higgs boson decaying to charm quarks”, *JHEP* **03** (2020) 131, doi:10.1007/JHEP03(2020)131, arXiv:1912.01662.
- [8] CMS Collaboration, “Search for Higgs boson decay to a charm quark-antiquark pair in proton-proton collisions at $\sqrt{s} = 13$ TeV”, *Phys. Rev. Lett.* **131** (2023) 061801, doi:10.1103/PhysRevLett.131.061801, arXiv:2205.05550.
- [9] CMS Collaboration, “Identification of heavy-flavour jets with the CMS detector in pp collisions at 13 TeV”, *JINST* **13** (2018) P05011, doi:10.1088/1748-0221/13/05/P05011, arXiv:1712.07158.
- [10] CMS Collaboration, “Identification of heavy, energetic, hadronically decaying particles using machine-learning techniques”, *JINST* **15** (2020) P06005, doi:10.1088/1748-0221/15/06/P06005, arXiv:2004.08262.
- [11] ATLAS Collaboration, “Direct constraint on the Higgs-charm coupling from a search for Higgs boson decays into charm quarks with the ATLAS detector”, *Eur. Phys. J. C* **82** (2022) 717, doi:10.1140/epjc/s10052-022-10588-3, arXiv:2201.11428.
- [12] H. Qu and L. Gouskos, “ParticleNet: Jet Tagging via Particle Clouds”, *Phys. Rev. D* **101** (2020) 056019, doi:10.1103/PhysRevD.101.056019, arXiv:1902.08570.

- [13] H. Qu, C. Li, and S. Qian, “Particle Transformer for jet tagging”, in *Proceedings of the 39th International Conference on Machine Learning*, pp. 18281–18292. 2022. [arXiv:2202.03772](#).
- [14] CMS Collaboration, “Transformer models for heavy flavor jet identification”, CMS Detector Performance Note CMS-DP-2022-050, 2022.
- [15] ATLAS Collaboration, “Graph Neural Network Jet Flavour Tagging with the ATLAS Detector”, ATLAS Note ATL-PHYS-PUB-2022-027, 2022.
- [16] CMS Collaboration, “Inclusive search for squarks and gluinos in pp collisions at $\sqrt{s} = 7$ TeV”, *Phys. Rev. D* **85** (2012) 012004, [doi:10.1103/PhysRevD.85.012004](#), [arXiv:1107.1279](#).
- [17] CMS Collaboration, “Search for supersymmetry with razor variables in pp collisions at $\sqrt{s}=7$ TeV”, *Phys. Rev. D* **90** (2014) 112001, [doi:10.1103/PhysRevD.90.112001](#), [arXiv:1405.3961](#).
- [18] ATLAS Collaboration, “Search for new phenomena in final states with large jet multiplicities and missing transverse momentum at $\sqrt{s}=8$ TeV proton-proton collisions using the ATLAS experiment”, *JHEP* **10** (2013) 130, [doi:10.1007/JHEP10\(2013\)130](#), [arXiv:1308.1841](#). [Erratum: *JHEP* 01, 109 (2014)].
- [19] B. Nachman et al., “Jets from Jets: Re-clustering as a tool for large radius jet reconstruction and grooming at the LHC”, *JHEP* **02** (2015) 075, [doi:10.1007/JHEP02\(2015\)075](#), [arXiv:1407.2922](#).
- [20] ATLAS Collaboration, “Jet reclustering and close-by effects in ATLAS run II”, ATLAS Note ATLAS-CONF-2017-062, CERN, Geneva, 2017.
- [21] E. Izaguirre, B. Shuve, and I. Yavin, “Improving Identification of Dijet Resonances at Hadron Colliders”, *Phys. Rev. Lett.* **114** (2015) 041802, [doi:10.1103/PhysRevLett.114.041802](#), [arXiv:1407.7037](#).
- [22] A. Banfi, G. P. Salam, and G. Zanderighi, “Principles of general final-state resummation and automated implementation”, *JHEP* **03** (2005) 073, [doi:10.1088/1126-6708/2005/03/073](#), [arXiv:hep-ph/0407286](#).
- [23] A. Vaswani et al., “Attention is All you Need”, in *Advances in Neural Information Processing Systems*, I. Guyon et al., eds., volume 30. Curran Associates, Inc., 2017.
- [24] CMS Collaboration, “Jet energy scale and resolution in the CMS experiment in pp collisions at 8 TeV”, *JINST* **12** (2017) P02014, [doi:10.1088/1748-0221/12/02/P02014](#), [arXiv:1607.03663](#).
- [25] ATLAS Collaboration, “Jet energy scale and resolution measured in proton–proton collisions at $\sqrt{s} = 13$ TeV with the ATLAS detector”, *Eur. Phys. J. C* **81** (2021) 689, [doi:10.1140/epjc/s10052-021-09402-3](#), [arXiv:2007.02645](#).
- [26] CMS Collaboration, “Calibration of the mass-decorrelated ParticleNet tagger for boosted $b\bar{b}$ and $c\bar{c}$ jets using LHC Run 2 data”, CMS Detector Performance Note CMS-DP-2022-005, 2022.

- [27] CMS Collaboration, “Performance of heavy-flavour jet identification in boosted topologies in proton-proton collisions at $\sqrt{s} = 13$ TeV”, CMS Physics Analysis Summary CMS-PAS-BTV-22-001, CERN, Geneva, 2023.
- [28] Y. Freund and R. E. Schapire, “A decision-theoretic generalization of on-line learning and an application to boosting”, *Journal of Computer and System Sciences* **55** (1997) 119, doi:<https://doi.org/10.1006/jcss.1997.1504>.
- [29] L. Breiman, J. Friedman, R. Olshen, and C. Stone, “Classification and Regression Trees”. Chapman and Hall/CRC, 1984.
- [30] ATLAS Collaboration, “Observation of $H \rightarrow b\bar{b}$ decays and VH production with the ATLAS detector”, *Phys. Lett. B* **786** (2018) 59–86, doi:[10.1016/j.physletb.2018.09.013](https://doi.org/10.1016/j.physletb.2018.09.013), arXiv:[1808.08238](https://arxiv.org/abs/1808.08238).
- [31] CMS Collaboration, “Observation of Higgs boson decay to bottom quarks”, *Phys. Rev. Lett.* **121** (2018) 121801, doi:[10.1103/PhysRevLett.121.121801](https://doi.org/10.1103/PhysRevLett.121.121801), arXiv:[1808.08242](https://arxiv.org/abs/1808.08242).
- [32] J. Alwall et al., “The automated computation of tree-level and next-to-leading order differential cross sections, and their matching to parton shower simulations”, *JHEP* **07** (2014) 079, doi:[10.1007/JHEP07\(2014\)079](https://doi.org/10.1007/JHEP07(2014)079), arXiv:[1405.0301](https://arxiv.org/abs/1405.0301).
- [33] T. Sjöstrand et al., “An introduction to PYTHIA 8.2”, *Comput. Phys. Commun.* **191** (2015) 159–177, doi:[10.1016/j.cpc.2015.01.024](https://doi.org/10.1016/j.cpc.2015.01.024), arXiv:[1410.3012](https://arxiv.org/abs/1410.3012).
- [34] J. Alwall et al., “Comparative study of various algorithms for the merging of parton showers and matrix elements in hadronic collisions”, *Eur. Phys. J. C* **53** (2008) 473–500, doi:[10.1140/epjc/s10052-007-0490-5](https://doi.org/10.1140/epjc/s10052-007-0490-5), arXiv:[0706.2569](https://arxiv.org/abs/0706.2569).
- [35] DELPHES 3 Collaboration, “DELPHES 3, A modular framework for fast simulation of a generic collider experiment”, *JHEP* **02** (2014) 057, doi:[10.1007/JHEP02\(2014\)057](https://doi.org/10.1007/JHEP02(2014)057), arXiv:[1307.6346](https://arxiv.org/abs/1307.6346).
- [36] M. Cacciari, G. P. Salam, and G. Soyez, “FastJet User Manual”, *Eur. Phys. J. C* **72** (2012) 1896, doi:[10.1140/epjc/s10052-012-1896-2](https://doi.org/10.1140/epjc/s10052-012-1896-2), arXiv:[1111.6097](https://arxiv.org/abs/1111.6097).
- [37] Particle Data Group Collaboration, “Review of Particle Physics”, *PTEP* **2022** (2022) 083C01, doi:[10.1093/ptep/ptac097](https://doi.org/10.1093/ptep/ptac097).
- [38] J. Dolen et al., “Thinking outside the ROCs: Designing Decorrelated Taggers (DDT) for jet substructure”, *JHEP* **05** (2016) 156, doi:[10.1007/JHEP05\(2016\)156](https://doi.org/10.1007/JHEP05(2016)156), arXiv:[1603.00027](https://arxiv.org/abs/1603.00027).
- [39] G. Louppe, M. Kagan, and K. Cranmer, “Learning to Pivot with Adversarial Networks”, arXiv:[1611.01046](https://arxiv.org/abs/1611.01046).
- [40] C. Shimmin et al., “Decorrelated Jet Substructure Tagging using Adversarial Neural Networks”, *Phys. Rev. D* **96** (2017) 074034, doi:[10.1103/PhysRevD.96.074034](https://doi.org/10.1103/PhysRevD.96.074034), arXiv:[1703.03507](https://arxiv.org/abs/1703.03507).
- [41] ATLAS Collaboration, “Performance of mass-decorrelated jet substructure observables for hadronic two-body decay tagging in ATLAS”, ATLAS Note ATL-PHYS-PUB-2018-014, 2018.

- [42] CMS Collaboration, “Identification of highly Lorentz-boosted heavy particles using graph neural networks and new mass decorrelation techniques”, CMS Detector Performance Note CMS-DP-2020-002, 2020.
- [43] L. Bradshaw, R. K. Mishra, A. Mitridate, and B. Ostdiek, “Mass Agnostic Jet Taggers”, *SciPost Phys.* **8** (2020) 011, doi:10.21468/SciPostPhys.8.1.011, arXiv:1908.08959.
- [44] G. Kasieczka and D. Shih, “Robust Jet Classifiers through Distance Correlation”, *Phys. Rev. Lett.* **125** (Sep, 2020) 122001, doi:10.1103/PhysRevLett.125.122001.
- [45] K. Benkendorfer, L. L. Pottier, and B. Nachman, “Simulation-assisted decorrelation for resonant anomaly detection”, *Phys. Rev. D* **104** (2021) 035003, doi:10.1103/PhysRevD.104.035003, arXiv:2009.02205.
- [46] O. Kitouni, B. Nachman, C. Weisser, and M. Williams, “Enhancing searches for resonances with machine learning and moment decomposition”, *Journal of High Energy Physics* **2021** (2021) 70, doi:10.1007/JHEP04(2021)070.
- [47] S. Klein and T. Golling, “Decorrelation with conditional normalizing flows”, arXiv:2211.02486.
- [48] CMS Collaboration, “Mass regression of highly-boosted jets using graph neural networks”, CMS Detector Performance Note CMS-DP-2021-017, 2021. CMS-DP-2021-017.
- [49] S. Mondal, G. Barone, and A. Schmidt, “PAIReD Jet Tagging Dataset”, May, 2024. doi:10.5281/zenodo.11150993, <https://doi.org/10.5281/zenodo.11150993>.
- [50] CMS Collaboration, “A new calibration method for charm jet identification validated with proton-proton collision events at $\sqrt{s} = 13$ TeV”, *JINST* **17** (2022) P03014, doi:10.1088/1748-0221/17/03/P03014, arXiv:2111.03027.
- [51] K. He, X. Zhang, S. Ren, and J. Sun, “Delving Deep into Rectifiers: Surpassing Human-Level Performance on ImageNet Classification”, *2015 IEEE International Conference on Computer Vision (ICCV)* (2015) 1026–1034.
- [52] Q. Wang, Y. Ma, K. Zhao, and Y. Tian, “A Comprehensive Survey of Loss Functions in Machine Learning”, *Annals of Data Science* **9** (2022) 187–212, doi:10.1007/s40745-020-00253-5.
- [53] T. Mikolov, “Statistical language models based on neural networks”. Ph.D. thesis, Brno University of Technology, Faculty of Information Technology, 2012.
- [54] H. Qu and C. Li, “weaver-core”. <https://pypi.org/project/weaver-core/>.
- [55] A. Paszke et al., “PyTorch: An Imperative Style, High-Performance Deep Learning Library”, in *Advances in Neural Information Processing Systems*, H. Wallach et al., eds., volume 32. Curran Associates, Inc., 2019.
- [56] L. Wright, “Ranger - a synergistic optimizer.”. <https://github.com/lessw2020/Ranger-Deep-Learning-Optimizer>, 2019.
- [57] P. Komiske, E. Metodiev, and J. Thaler, “Pythia8 Quark and Gluon Jets for Energy Flow”, May, 2019. doi:10.5281/zenodo.3164691, <https://doi.org/10.5281/zenodo.3164691>.

- [58] G. Kasieczka, T. Plehn, J. Thompson, and M. Russel, “Top quark tagging reference dataset”, March, 2019. doi:10.5281/zenodo.2603256, <https://doi.org/10.5281/zenodo.2603256>.
- [59] H. Qu, C. Li, and S. Qian, “JetClass: A large-scale dataset for deep learning in jet physics”, 2022. doi:10.5281/zenodo.6619768, <https://doi.org/10.5281/zenodo.6619768>.
- [60] Y. Chen et al., “A FAIR and AI-ready Higgs boson decay dataset”, *Scientific Data* **9** (2022) 31, doi:10.1038/s41597-021-01109-0.
- [61] J. H. Friedman, “Greedy function approximation: A gradient boosting machine.”, *The Annals of Statistics* **29** (2001) 1189 – 1232, doi:10.1214/aos/1013203451.
- [62] T. Chen and C. Guestrin, “XGBoost: A Scalable Tree Boosting System”, in *Proceedings of the 22nd ACM SIGKDD International Conference on Knowledge Discovery and Data Mining*, KDD ’16. ACM, August, 2016. doi:10.1145/2939672.2939785.
- [63] G. Van Rossum and F. L. Drake, “Python 3 Reference Manual”. CreateSpace, Scotts Valley, CA, 2009. ISBN 1441412697.
- [64] F. Pedregosa et al., “Scikit-learn: Machine learning in Python”, *Journal of Machine Learning Research* **12** (2011) 2825–2830.
- [65] J. Erdmann et al., “A likelihood-based reconstruction algorithm for top-quark pairs and the KLFitter framework”, *Nucl. Instrum. Meth. A* **748** (2014) 18–25, doi:10.1016/j.nima.2014.02.029, arXiv:1312.5595.
- [66] J. Erdmann, T. Kallage, K. Kröniger, and O. Nackenhorst, “From the bottom to the top—reconstruction of $t\bar{t}$ events with deep learning”, *JINST* **14** (2019) P11015, doi:10.1088/1748-0221/14/11/P11015, arXiv:1907.11181.
- [67] A. Shmakov et al., “SPANet: Generalized permutationless set assignment for particle physics using symmetry preserving attention”, *SciPost Phys.* **12** (2022), no. 5, 178, doi:10.21468/SciPostPhys.12.5.178, arXiv:2106.03898.
- [68] A. J. Larkoski, S. Marzani, G. Soyez, and J. Thaler, “Soft Drop”, *JHEP* **05** (2014) 146, doi:10.1007/JHEP05(2014)146, arXiv:1402.2657.
- [69] CMS Collaboration, “A Deep Neural Network for Simultaneous Estimation of b Jet Energy and Resolution”, *Comput. Softw. Big Sci.* **4** (2020) 10, doi:10.1007/s41781-020-00041-z, arXiv:1912.06046.
- [70] CERN, “CERN Yellow Reports: Monographs, Vol 2 (2017): Handbook of LHC Higgs cross sections: 4. Deciphering the nature of the Higgs sector”, 2017. doi:10.23731/CYRM-2017-002, <https://e-publishing.cern.ch/index.php/CYRM/issue/view/32>.
- [71] Y. L. Dokshitzer, G. D. Leder, S. Moretti, and B. R. Webber, “Better jet clustering algorithms”, *JHEP* **08** (1997) 001, doi:10.1088/1126-6708/1997/08/001, arXiv:hep-ph/9707323.

- [72] M. Wobisch and T. Wengler, “Hadronization corrections to jet cross-sections in deep inelastic scattering”, in *Workshop on Monte Carlo Generators for HERA Physics (Plenary Starting Meeting)*, pp. 270–279. 4, 1998. [arXiv:hep-ph/9907280](#).
- [73] Y. S. Lai, J. Mulligan, M. Płoskoń, and F. Ringer, “The information content of jet quenching and machine learning assisted observable design”, *JHEP* **10** (2022) 011, [doi:10.1007/JHEP10\(2022\)011](#), [arXiv:2111.14589](#).
- [74] Y. Lu et al., “Resolving extreme jet substructure”, *JHEP* **08** (2022) 046, [doi:10.1007/JHEP08\(2022\)046](#), [arXiv:2202.00723](#).
- [75] D. Athanasakos et al., “Is infrared-collinear safe information all you need for jet classification?”, [arXiv:2305.08979](#).
- [76] D. Bertolini, P. Harris, M. Low, and N. Tran, “Pileup Per Particle Identification”, *JHEP* **10** (2014) 059, [doi:10.1007/JHEP10\(2014\)059](#), [arXiv:1407.6013](#).
- [77] P. T. Komiske, E. M. Metodiev, B. Nachman, and M. D. Schwartz, “Pileup Mitigation with Machine Learning (PUMML)”, *JHEP* **12** (2017) 051, [doi:10.1007/JHEP12\(2017\)051](#), [arXiv:1707.08600](#).
- [78] P. Hansen, J. W. Monk, and C. Wiglesworth, “A Wavelet Based Pile-Up Mitigation Method for the LHC Upgrade”, [arXiv:1812.07412](#).
- [79] J. Arjona Martínez et al., “Pileup mitigation at the Large Hadron Collider with graph neural networks”, *Eur. Phys. J. Plus* **134** (2019) 333, [doi:10.1140/epjp/i2019-12710-3](#), [arXiv:1810.07988](#).
- [80] S. Alipour-fard, P. T. Komiske, E. M. Metodiev, and J. Thaler, “Pileup and Infrared Radiation Annihilation (PIRANHA): A Paradigm for Continuous Jet Grooming”, [arXiv:2305.00989](#).
- [81] I. W. Stewart et al., “XCone: N-jettiness as an Exclusive Cone Jet Algorithm”, *JHEP* **11** (2015) 072, [doi:10.1007/JHEP11\(2015\)072](#), [arXiv:1508.01516](#).
- [82] J. Thaler and T. F. Wilkason, “Resolving Boosted Jets with XCone”, *JHEP* **12** (2015) 051, [doi:10.1007/JHEP12\(2015\)051](#), [arXiv:1508.01518](#).
- [83] T. Lapsien, R. Kogler, and J. Haller, “A new tagger for hadronically decaying heavy particles at the LHC”, *Eur. Phys. J. C* **76** (2016) 600, [doi:10.1140/epjc/s10052-016-4443-8](#), [arXiv:1606.04961](#).
- [84] B. Mukhopadhyaya, T. Samui, and R. K. Singh, “Dynamic radius jet clustering algorithm”, *JHEP* **04** (2023) 019, [doi:10.1007/JHEP04\(2023\)019](#), [arXiv:2301.13074](#).
- [85] A. J. Larkoski, D. Rathjens, J. Veatch, and J. W. Walker, “Jet SIFT-ing: a new scale-invariant jet clustering algorithm for the substructure era”, [arXiv:2302.08609](#).
- [86] X. Ju and B. Nachman, “Supervised Jet Clustering with Graph Neural Networks for Lorentz Boosted Bosons”, *Phys. Rev. D* **102** (2020) 075014, [doi:10.1103/PhysRevD.102.075014](#), [arXiv:2008.06064](#).

A Mass regression

Before flavor classifiers are trained (cf. Sec. 5), regression networks are trained to define a regressed jet mass for AK8, AK15, PAIReD, and PAIReDEllipse jets. The same ParT architecture, with some modifications (cf. Sec. 4), is used. Defining a jet mass is necessary so that the classification networks can be trained to be uncorrelated with respect to this mass quantity [42]. While regular mass terms like SoftDropped mass [68] can be used in the case of AK8 and AK15 jets, they are not well-defined for jets that do not have a characteristic jet radius (the soft-drop condition requires a radius parameter R_0 , see Ref. [68]) such as the PAIReD and PAIReDEllipse jets. Therefore, for a fair comparison in subsequent steps, the regressed mass (m_{reg}) is devised as a mass term that can be uniformly defined for all four kinds of jets. Moreover, using the same technique to regress mass values for all reconstruction strategies allows us to compare the accuracy and resolution of the jet mass across all strategies.

A mass regression network is trained each for AK8, AK15, PAIReD, and PAIReDEllipse jets. Jets with labels bb and cc (cf. Sec. 3) sampled from the flat-mass $\text{ZH}(\text{H} \rightarrow \text{b}\bar{\text{b}})$ and $\text{ZH}(\text{H} \rightarrow \text{c}\bar{\text{c}})$ processes are used in the training. The mass of the generated Higgs boson is set as the target of the regression. The jets are further assigned weights to ensure that the distribution of the generated Higgs boson mass is flat in the entire range of 10–500 GeV.

About 13–15 million jets with label bb, and a similar number of jets with label cc, are used in the training process. The exact number varies across reconstruction strategies. About 90% of these jets are used in the training while the remaining are used as an independent validation dataset to avoid overtraining. Each training is run for 50 epochs, which is deemed enough for the training to converge. The model from the epoch with the lowest validation loss is chosen as the final regression model.

The trainings are evaluated on an independent test dataset comprising jets from $\text{ZH}(\text{H} \rightarrow \text{b}\bar{\text{b}})$ and $\text{ZH}(\text{H} \rightarrow \text{c}\bar{\text{c}})$ processes with $m_{\text{H}} = 125$ GeV, and Z+jj processes. The evaluation results for the PAIReDEllipse jet training are shown in Fig. 8 as an example. As expected, the distribution of m_{reg} peaks at around the Higgs boson mass for the bb and cc samples. A Double-sided Crystal Ball (DCB) fit is performed to extract the mean and spread of these distributions. A mass resolution of about 15 GeV is obtained. The distribution of m_{reg} assumes a smoothly falling shape for ll jets taken from Z+jj processes, as expected.

It was observed that the mean and spread of the m_{reg} distribution had a moderate dependence on the generated Higgs boson p_{T} . The mass distributions were hence plotted for different ranges of the generated Higgs boson p_{T} and the DCB fit was performed separately for every range. The mean and spread parameters obtained from the fits are plotted as functions of the generated Higgs boson p_{T} in Fig. 9. In general, a better mass resolution is obtained at higher values of the Higgs boson p_{T} . In all cases, the mean is compatible with the true mass of 125 GeV within the respective resolutions.

Figure 9 also shows the fit results for the dijet invariant mass in signal events using the AK4-based reconstruction strategy, for reference. The AK4-based strategy exhibits a poorer mass resolution compared to other strategies employing dedicated mass regression techniques. However, a better mass resolution in AK4-based reconstruction is usually achieved in physics analyses [8, 31] using

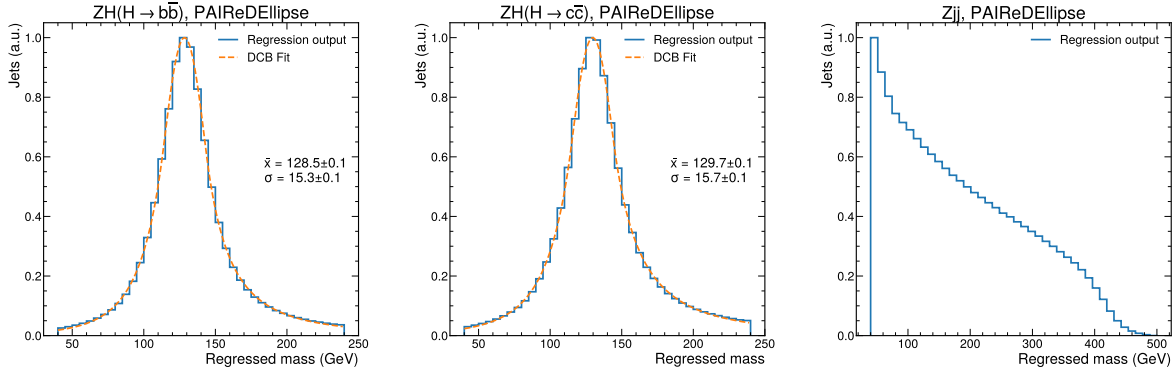


Figure 8: The distribution of the regressed mass obtained from the PAIReDEllipse jet regression training evaluated on bb jets from $ZH(H \rightarrow b\bar{b})$ (left), cc jets from $ZH(H \rightarrow c\bar{c})$ (center), and light-flavor jets from $Z+jj$ (right) processes. The blue histograms represent the network outputs, while the orange lines in the first two plots show the results of a Double-sided Crystal Ball (DCB) fit. The mean (\bar{x}) and spread (σ) parameters of the fit are also displayed on the first two plots. The distributions are truncated between 40–240 GeV for bb and cc jets, and 40–500 GeV for ll jets.

techniques like b and c jet mass regression [69] that evaluate per-jet corrections. Such techniques have not been used in this paper.

The PAIReD approach achieves the best mass resolution at lower Lorentz-boosts of the generated Higgs boson. The PAIReDEllipse approach has a slightly poorer resolution, since PAIReDEllipse jets are expected to contain a larger number of reconstructed particles from pileup and unrelated hadronic activities compared to the PAIReD approach at high opening angles. The AK8 and AK15 approaches either do not yield sufficient jets or have a poor mass resolution at low boosts. This is because they fail to encompass the full decay at low p_T 's. On the other hand, the PAIReDEllipse, AK8, and AK15 approaches exhibit similar mass resolutions at high Lorentz-boosts.

To validate whether the jet flavor tagging classifiers trained in this study introduce artificial peaks in the mass spectrum of background jets—a phenomenon referred to as mass sculpting—the distribution of m_{reg} is plotted for background jets that satisfy a tight selection criterion in the classifier output score. Figure 10 (right) shows the m_{reg} spectrum of background jets corresponding to various reconstruction strategies at a fixed ll mistag rate of 1% achieved by the respective classifier, along with the corresponding pre-selection distributions for reference. While the application of a selection criterion on the tagger score moderately affects the overall m_{reg} distribution, it does not induce artificial peaks in the background mass spectrum and the distribution continues to have a smooth decline with increasing mass. On the other hand, the signal jets shown in Fig. 10 (left) have a mass spectrum that sharply peaks at around the Higgs mass and remains unchanged upon the application of tagger selections. Therefore, the signal and background jets maintain a separation in their mass spectra even after selections on classifier scores are applied. This ensures a fair comparison among these strategies, as well as between these strategies and the inherently mass-agnostic AK4-based reconstruction approach.

The mass regression technique was also applied on Cone15 jets (cf. Appendix F.2). The results of the DCB fit to the regressed masses for AK15 and Cone15 jets are shown in Fig. 11. The mass

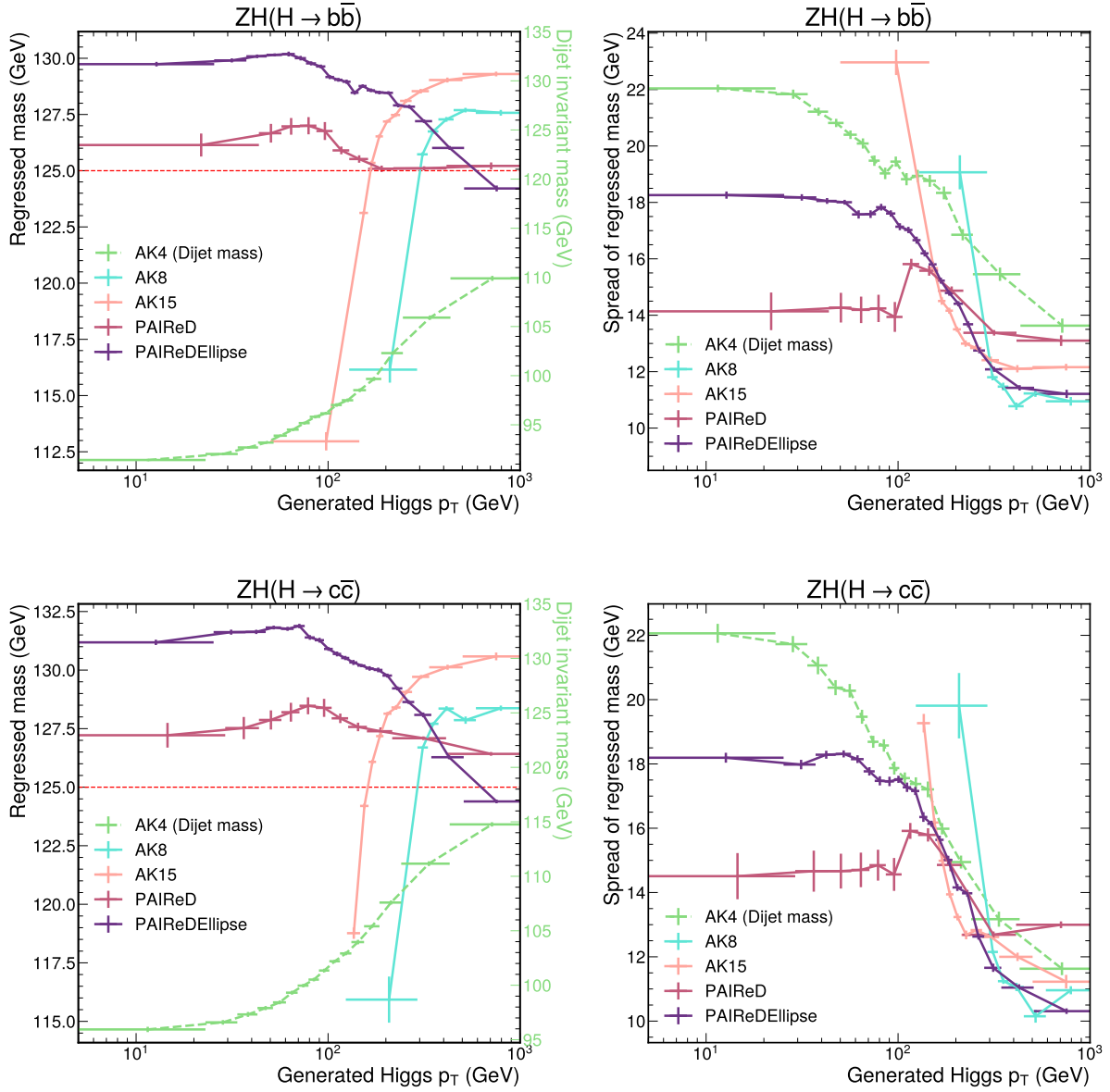


Figure 9: The mean (left) and spread (right) fit parameters of the regressed mass as a function of the generated Higgs boson p_T for different reconstruction strategies are shown. Uncertainty bands indicate fit uncertainties. The binning for each strategy is chosen in a way such that each bin contains approximately an equal number of jets. The upper (lower) row shows results for $b\bar{b}$ ($c\bar{c}$) jets taken from $ZH(H \rightarrow b\bar{b})$ ($ZH(H \rightarrow c\bar{c})$) processes. The fit results of the dijet invariant mass (the light-green dashed lines) are also shown for the AK4-based reconstruction strategy. The corresponding y-axis is shown on the right edge of the mean plot (left) in light-green text.

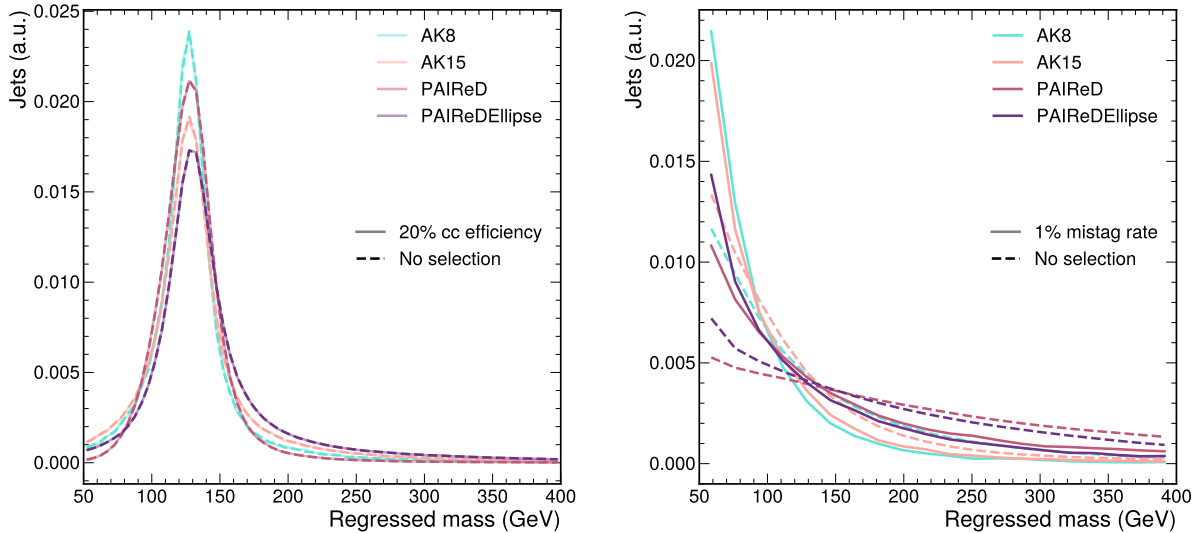


Figure 10: The distribution of the regressed mass of the cc signal (left) and ll background (right) jets before (the dashed lines) and after (the solid lines) a selection criterion is applied on the output scores of different classifiers. The selection criteria are chosen such that exactly 20% (1%) of the signal (background) jets are selected in each case. All curves are individually normalized to unity. In the left plot, the pre- and post-selection curves for the same kind of jet overlap.

resolutions obtained from the two methods are similar. Regression using the Cone15 approach, however, yields means closer to the generated Higgs boson mass both at low and high boosts of the Higgs boson.

B Differential signal sensitivity (S/\sqrt{B}) in a $ZH(H \rightarrow c\bar{c})$ analysis

We define a signal sensitivity metric as the ratio of the number of selected signal events (S) to the square-root of the number of passing background events (B) after all selection criteria and classifier score requirements are applied (cf. Sec. 6). This can be evaluated at a target end-to-end signal efficiency value, as well as across various reconstruction strategies. As discussed in Sec. 3, only the major background ($Z+jj$) has been considered in this study. To estimate the approximate signal and background yields, the $ZH(H \rightarrow c\bar{c})$ and $Z+jj$ processes are assigned cross sections of 0.0027 and 270 pb, respectively. The former value is taken from the LHC Higgs Cross Section Working Group report [70], while the latter is obtained from PYTHIA8 after MLM matching is performed during the sample generation. The simulations are scaled to an integrated luminosity of 200 fb^{-1} , corresponding to the expected data to be delivered by the LHC in Run-3.

The S/\sqrt{B} values for four different target signal efficiencies are shown in Fig. 12. The signal and background yields in each bin are normalized to reflect a fixed Higgs/diparton p_T range, specifically a range of 10 GeV, so that the S/\sqrt{B} value is independent of the choice of bin width.

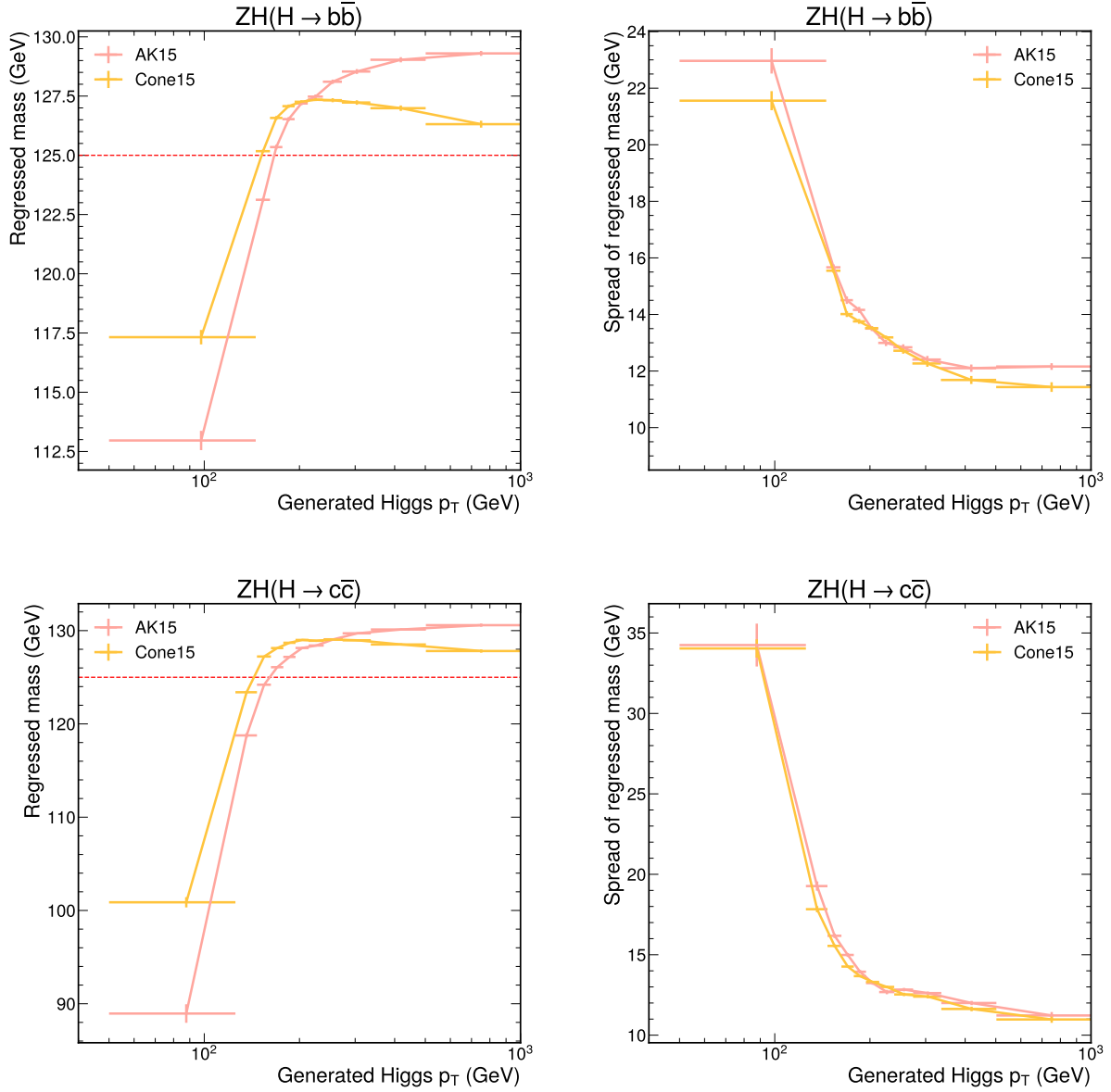


Figure 11: The mean (left) and spread (right) fit parameters of the regressed mass as a function of the generated Higgs boson p_T for AK15 and Cone15 jets are shown. Uncertainty bands indicate fit uncertainties. The upper (lower) row shows results for $b\bar{b}$ ($c\bar{c}$) jets taken from $ZH(H \rightarrow b\bar{b})$ ($ZH(H \rightarrow c\bar{c})$) processes.

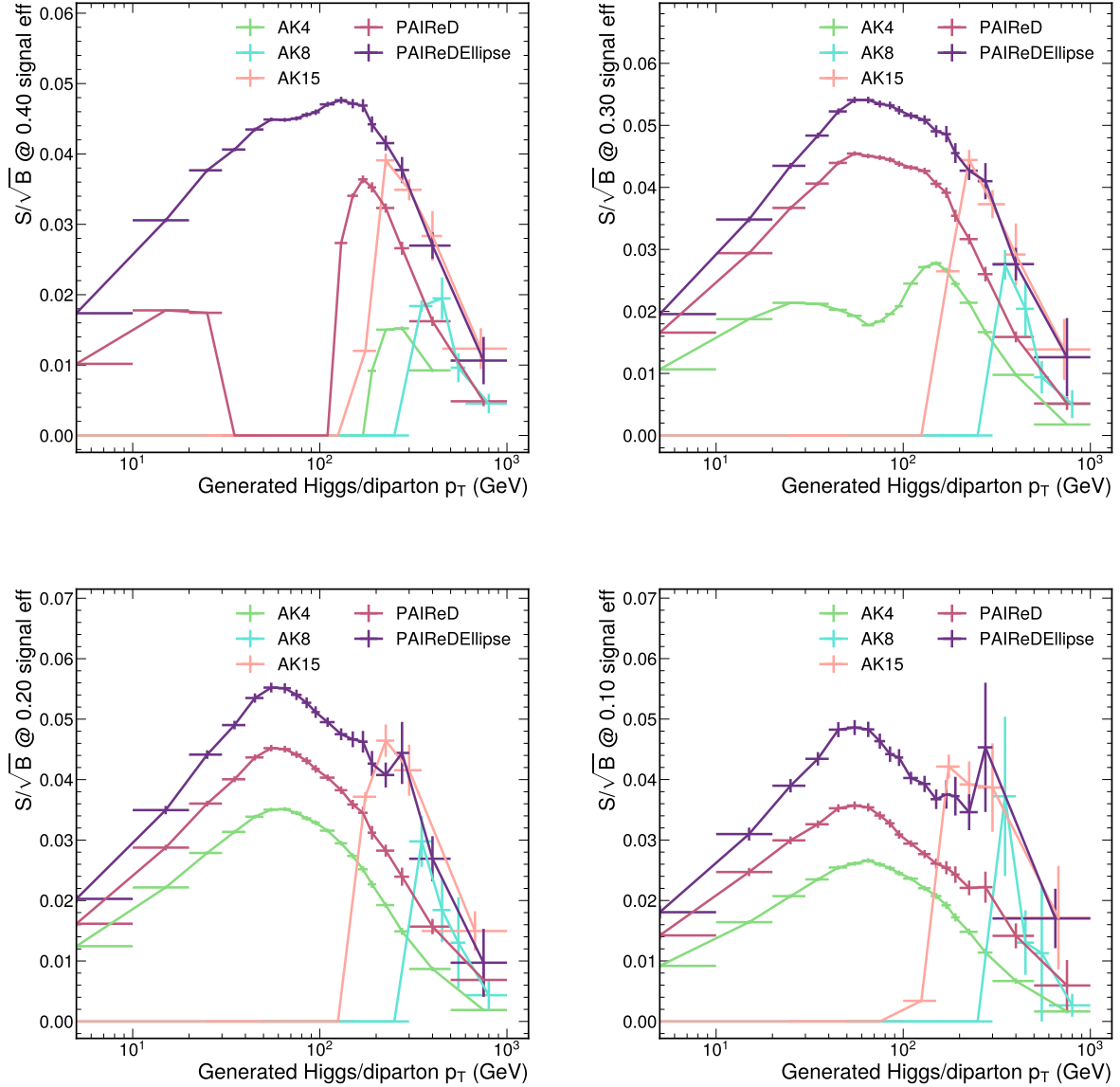


Figure 12: The S/\sqrt{B} values at end-to-end signal efficiencies of 0.4 (upper-left), 0.3 (upper-right), 0.2 (lower-left), and 0.1 (lower-right) as a function of the generated Higgs boson p_T (for signal) or diparton p_T (for background), plotted for various reconstruction strategies. Signal and background yields in each bin are normalized to reflect a fixed Higgs/diparton p_T range of 10 GeV. The target end-to-end signal efficiencies are calculated per bin. The S/\sqrt{B} value is set to 0 wherever target signal efficiency cannot be achieved.

The trends observed in Fig. 12 closely follow those observed in Fig. 6. At low Lorentz-boosts, the PAIReDEllipse strategy achieves up to twice the signal sensitivity that the AK4-based strategy achieves, while the PAIReD strategy has an intermediate performance. At higher boosts, the PAIReDEllipse and AK15 strategies have similar performances. The maximum S/\sqrt{B} is achieved in Higgs boson p_T ranges of 50–80 GeV at per-bin signal efficiencies of 0.2–0.3, using the PAIReDEllipse strategy. This reinforces the hypothesis that novel reconstruction and tagging strategies employed at the resolved-jet regime can significantly improve the overall sensitivity of such analyses. However, these studies rely only on the major background simulation and do not consider any systematic uncertainties, and can therefore be regarded as rough estimates only.

C Event-level BDT performance at different Higgs p_T and jet multiplicities

The performance of the event-level BDTs described in Sec. 6.3.4 is further evaluated as a function of the Higgs/diparton p_T . The end-to-end background rejection rates achieved at end-to-end signal efficiencies of 0.4, 0.3, 0.2, and 0.1 are shown in Fig. 13.

The overall background rejections achieved at a given signal efficiency are higher compared to the corresponding values in Fig. 6. This is expected since the BDT is able to leverage more event-level information in addition to the tagger scores. The trends across reconstruction strategies, however, remain similar, with the BDT trained with PAIReDEllipse jet scores rejecting about 2–2.5 times more background events compared to the BDT trained with AK4 jet scores (as opposed to a 2.5–4 times improvement reported in the case of tagger-only discrimination in Sec. 6.3.3). This reflects the fact that an event-level BDT in case of the AK4 jet-based reconstruction approach can partially account for correlations between two jets by leveraging the tagger scores of the two jets (4 additional inputs, as shown in Tab. 2). However, this still falls short of the performance achievable using event-level BDTs with the PAIReD(Ellipse) approaches, as the latter leverage additional information and correlations at the jet constituent level that are inaccessible to AK4-based taggers.

The performance of the BDTs are also evaluated for different jet multiplicities. The corresponding ROC curves are shown in Fig. 14. It is observed that the classification performance using PAIReD(Ellipse) jets does not drop significantly at low boosts despite the higher combinatorial complexity. In fact, events with high small-radius jet multiplicities (and consequently high PAIReD(Ellipse) jet multiplicities) play a significant role especially at high boosts of the Higgs boson.

D Validation with $ZZ(Z \rightarrow c\bar{c})$ analysis

Additional $ZZ(Z \rightarrow c\bar{c})$ processes are simulated as per the description in Sec. 3, with the difference that the $Z \rightarrow c\bar{c}$ decay is performed in MG5 instead of PYTHIA8. A mock $ZZ(Z \rightarrow c\bar{c})$ analysis is designed in a way similar to the $ZH(H \rightarrow c\bar{c})$ analysis described in Sec. 6.

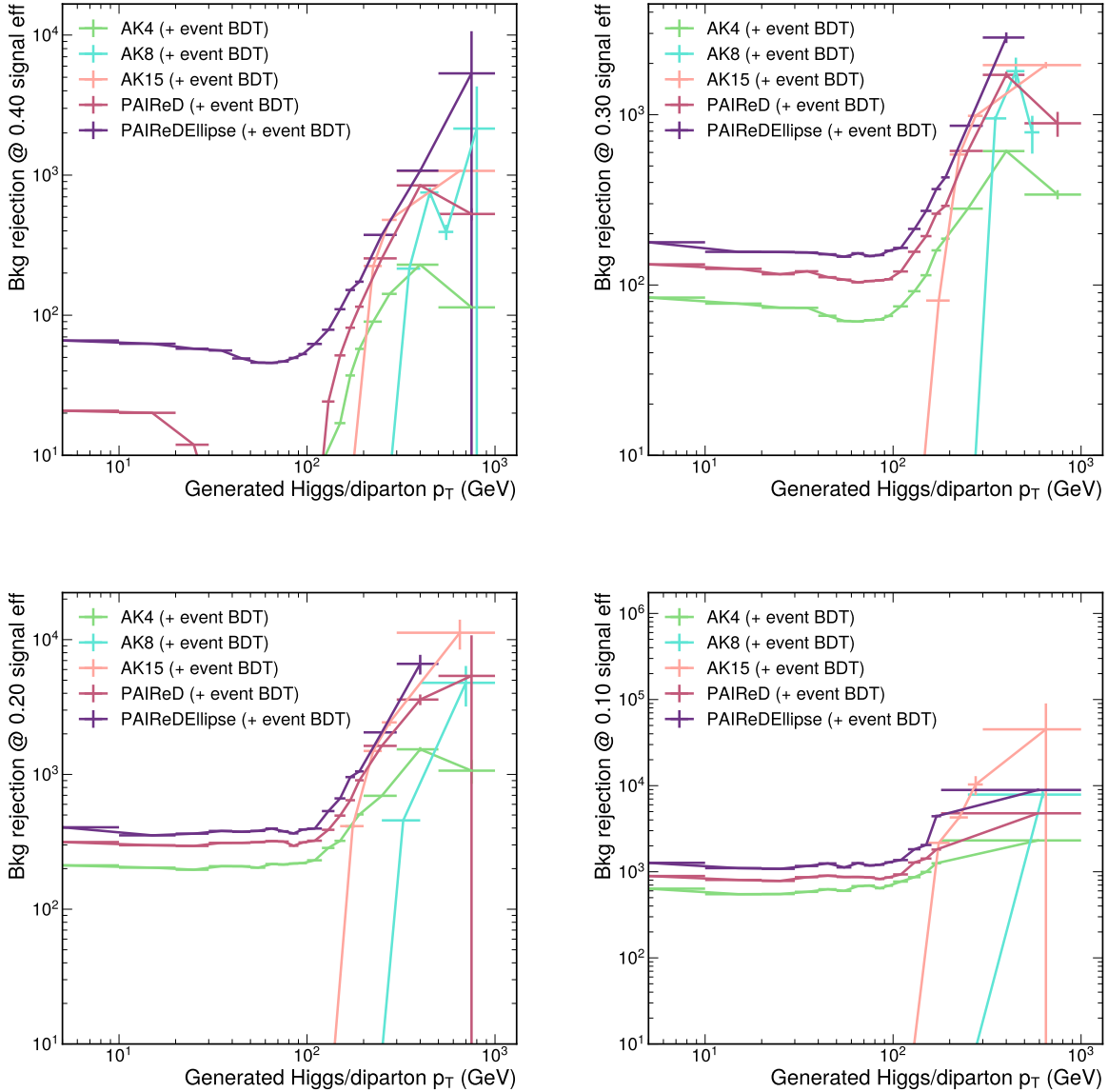


Figure 13: The end-to-end background rejection at end-to-end signal efficiencies of 0.4 (upper-left), 0.3 (upper-right), 0.2 (lower-left), and 0.1 (lower-right) as a function of the generated Higgs boson p_T (for signal) or diparton p_T (for background) achieved with event-level BDTs (cf. Sec. 6.3.4), plotted for various reconstruction strategies. End-to-end signal efficiencies and background rejections are calculated per bin. The background rejection is set to 0 wherever the target signal efficiency cannot be achieved. Bins with very low yield of background events are either merged with adjacent bins or are omitted. Compared to Fig. 6, bin widths and statistical uncertainties are larger in this figure as the number of events used is approximately half.

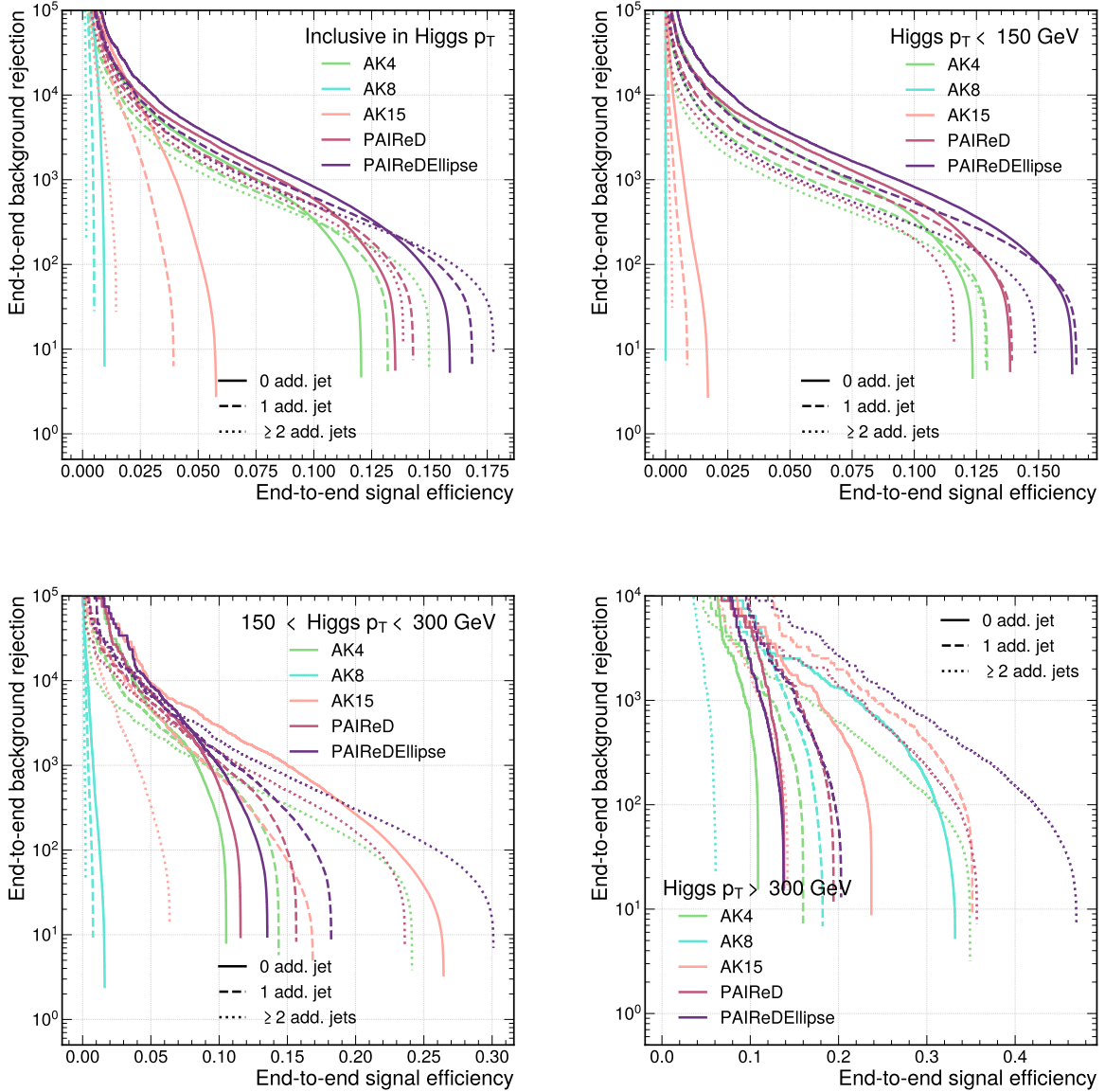


Figure 14: The end-to-end background event rejection rate as a function of the end-to-end signal efficiency inclusively in Higgs boson (or diparton) p_T (upper-left), at low ($p_T < 150$ GeV) p_T ranges (upper-right), at medium ($150 < p_T < 300$ GeV) p_T ranges (lower-left), and at high ($p_T > 300$ GeV) p_T ranges (lower-right), across different jet multiplicities, as predicted by the event-level BDT. The solid lines represent events with exactly 2 AK4 jets, 1 AK8/AK15 jet, or 1 PAIReD/PAIReDEllipse jet. The dashed lines represent events with exactly 3 AK4 jets, 2 AK8/AK15 jets, or 3 PAIReD/PAIReDEllipse jets. The dotted lines represent events with at least 4 AK4 jets, 3 AK8/AK15 jets, or 6 PAIReD/PAIReDEllipse jets. The highest value along the x-axis reached by each curve represents the maximum signal reconstruction efficiency (w.r.t. the total number of generated events, irrespective of the number of reconstructable jets) achievable using the respective event reconstruction strategy (cf. Sec. 6.3.1) with the respective number of reconstructed jets.

The mass regression trainings obtained from using the Higgs boson samples are used to predict the regressed mass values of the hadronically-decaying Z boson in the $ZZ(Z \rightarrow c\bar{c})$ samples. The regressed mass and its spread for different reconstruction strategies are shown in Fig. 15. The decay width of the Z boson ($\Gamma_Z \approx 2.5$ GeV [37]) is neglected as it is small compared to the best mass resolution ($\sigma_Z \approx 8$ GeV) achieved using this method ($\Gamma_Z^2 \ll \sigma_Z^2$). The relative mass resolution (σ/\bar{x}) values are consistent with the ones obtained for the Higgs boson sample (Fig. 9).

Similarly, the existing classifier trainings are used to perform the $ZZ(Z \rightarrow c\bar{c})$ analysis. The signal reconstruction efficiencies and the classifier AUCs as a function of the hadronic Z boson (or diparton) p_T are shown in Fig. 16. The background rejection and differential signal sensitivity estimates (S/\sqrt{B}) at different values of the end-to-end signal efficiencies are shown in Figs. 17 and 18, respectively. A cross section of 0.155 pb is used for the $ZZ(Z \rightarrow c\bar{c})$ process. This cross section is predicted by PYTHIA8 after MLM jet matching is performed.

The trends observed in the $ZZ(Z \rightarrow c\bar{c})$ analysis closely follow those observed in the $ZH(H \rightarrow c\bar{c})$ analysis. The overall signal efficiency is lower in case of the $ZZ(Z \rightarrow c\bar{c})$ analysis owing to the regressed mass (or dijet invariant mass) requirement of $m_{\text{reg}} \in [50, 200]$ GeV, tuned for the Higgs boson analysis. However, the observations highlight the generalizability of the reconstruction algorithms and classifier trainings to a wider set of final states.

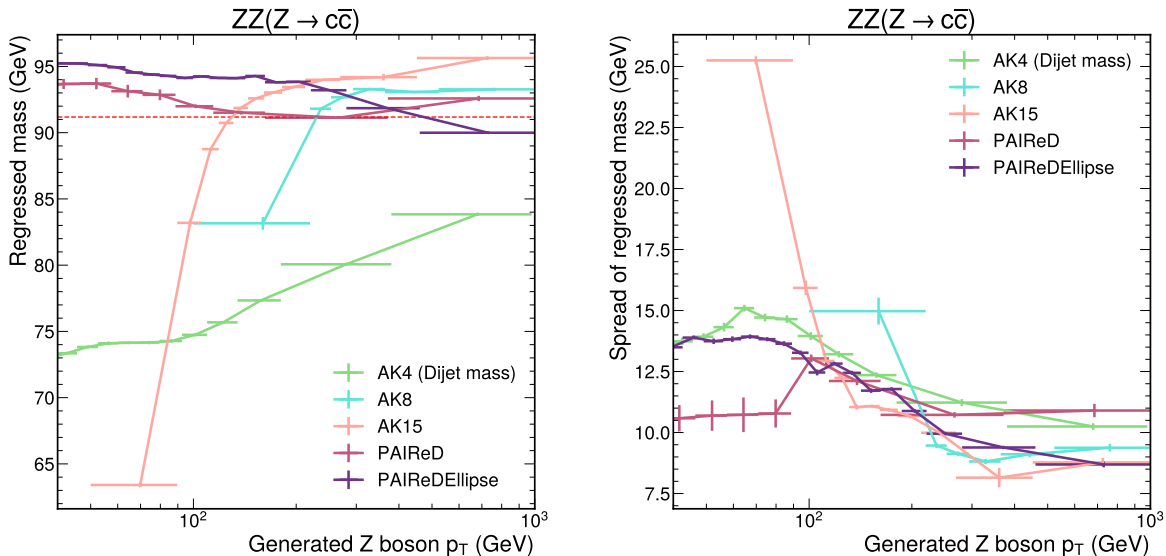


Figure 15: The mean (left) and spread (right) fit parameters of the regressed mass as a function of the generated Z boson p_T for different reconstruction strategies are shown. Uncertainty bands indicate fit uncertainties. The binning for each strategy is chosen in a way such that each bin contains approximately an equal number of jets. The cc jets from the $ZZ(Z \rightarrow c\bar{c})$ processes are used. The y-axis indicates the dijet invariant mass for the AK4-based reconstruction strategy.

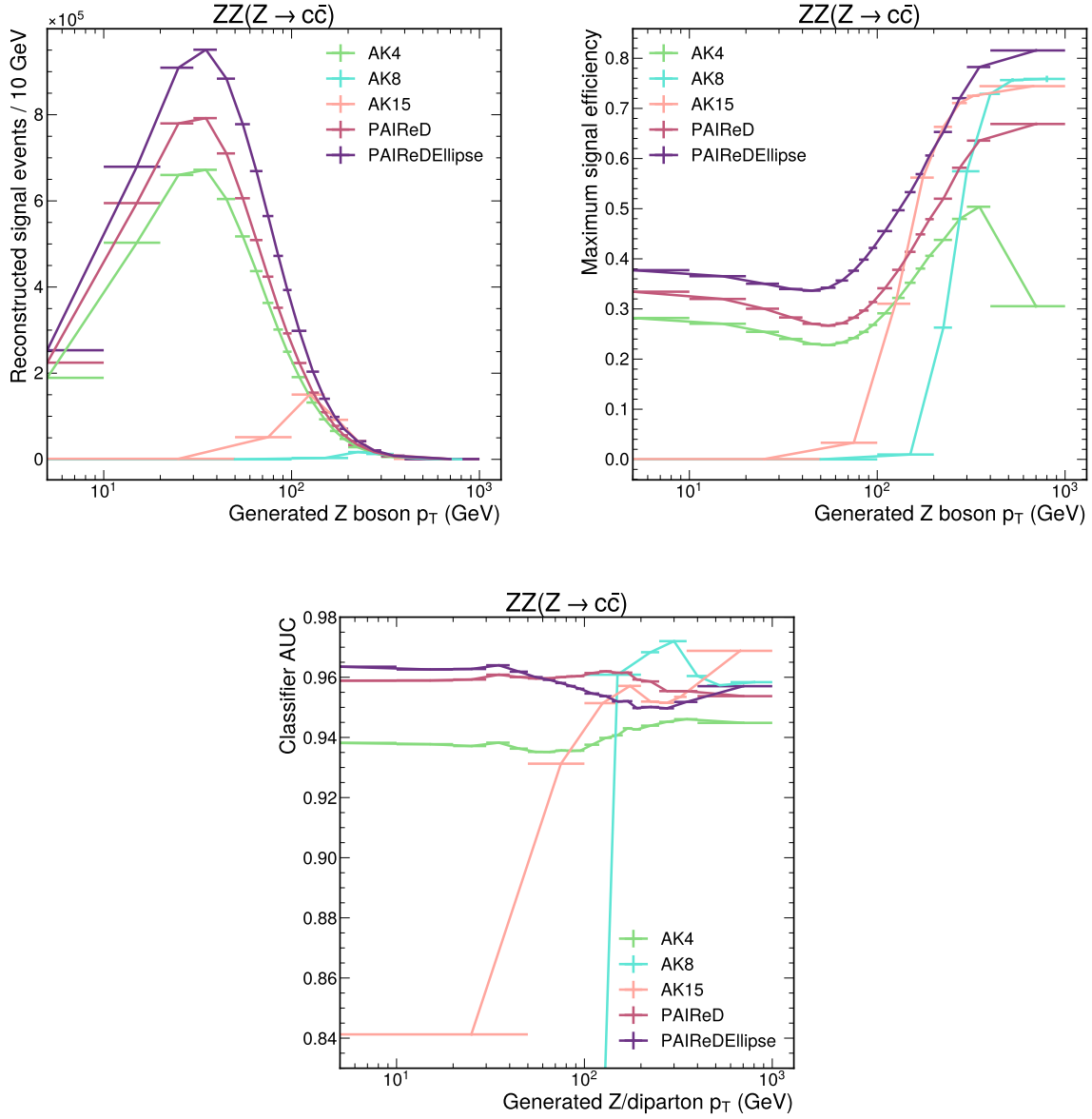


Figure 16: The number of reconstructed $ZZ(Z \rightarrow c\bar{c})$ signal events out of the ~ 11 M signal events generated (upper left) and the maximum signal efficiency or the signal reconstruction efficiency (upper right) as functions of the generated Z boson p_T , for various reconstruction strategies. The lower plot shows the area under the ROC curves (AUC) obtained when classifiers corresponding to various reconstruction strategies are evaluated on the signal and background events passing the respective selections, plotted as a function of the Z boson p_T (for signal events) or the diparton p_T (for background events).

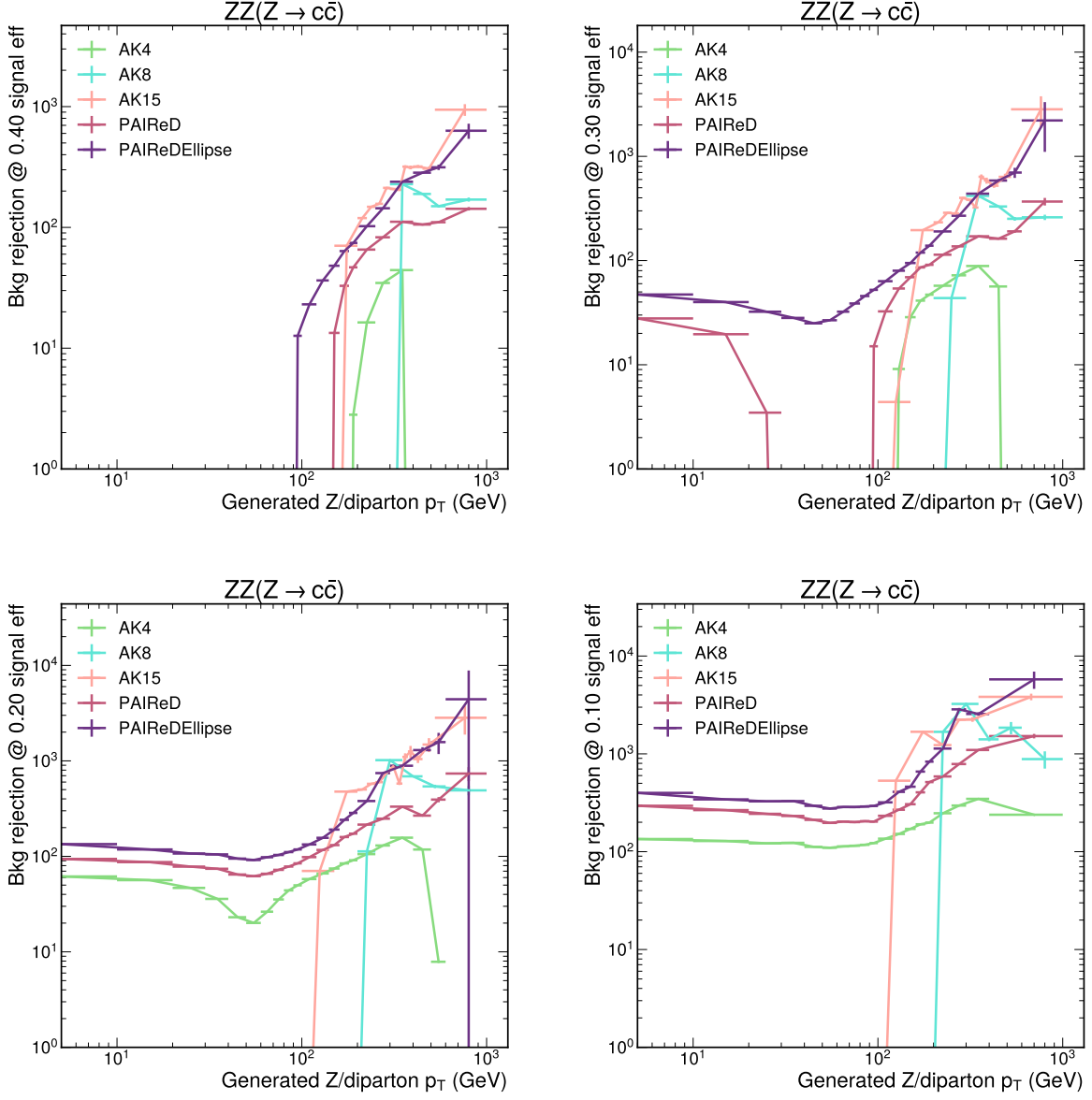


Figure 17: The end-to-end background rejection at end-to-end signal efficiencies of 0.4 (upper-left), 0.3 (upper-right), 0.2 (lower-left), and 0.1 (lower-right) as a function of the generated Z p_T (for signal) or diparton p_T (for background), plotted for various reconstruction strategies. End-to-end signal efficiencies and background rejections are calculated per bin. The background rejection is set to 0 wherever the target signal efficiency cannot be achieved. Bins with very low yield of background events are either merged with adjacent bins or are omitted.

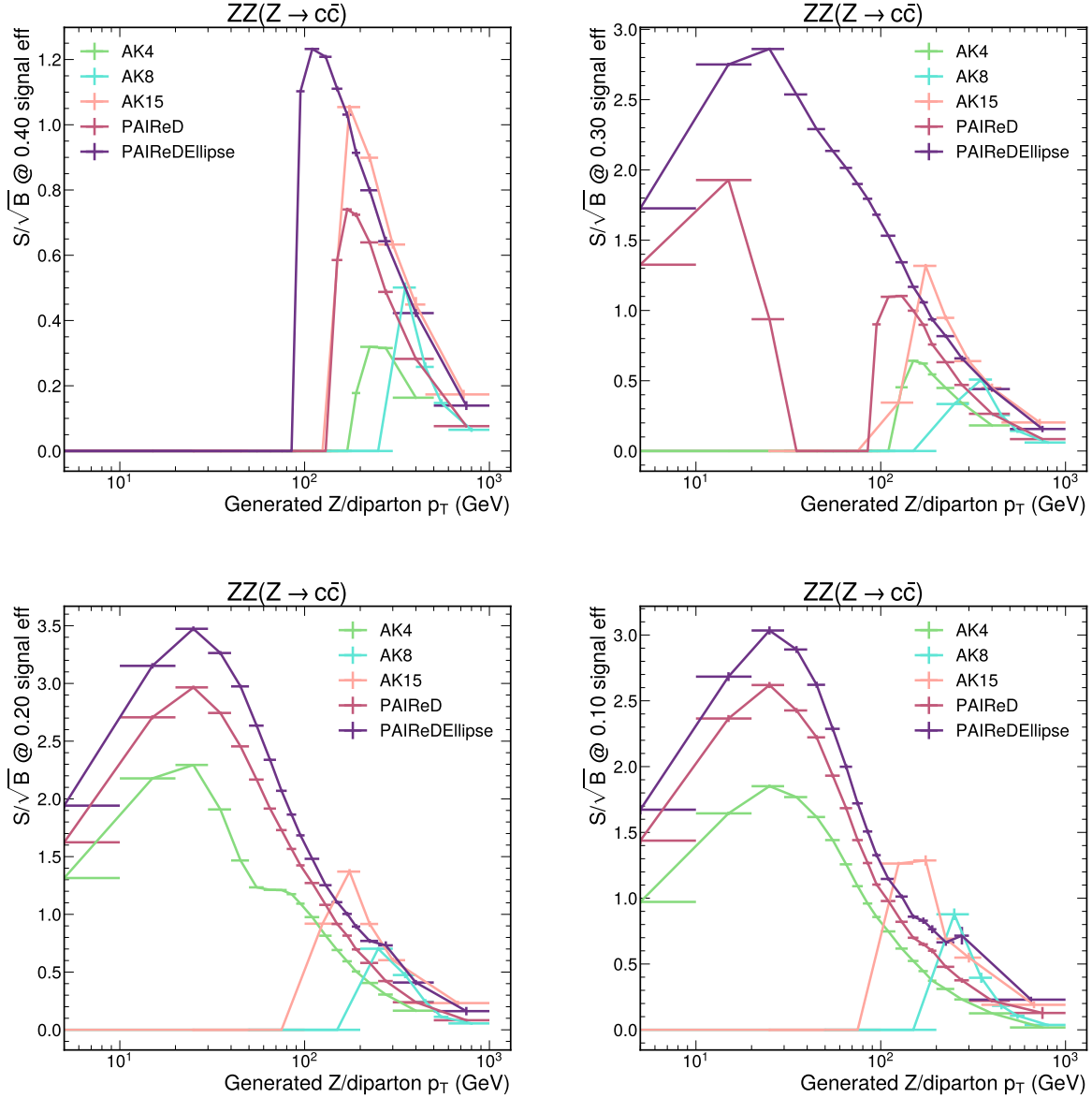


Figure 18: The S/\sqrt{B} values at end-to-end signal efficiencies of 0.4 (upper-left), 0.3 (upper-right), 0.2 (lower-left), and 0.1 (lower-right) as a function of the generated Z boson p_T (for signal) or diparton p_T (for background), plotted for various reconstruction strategies. Signal and background yields in each bin are normalized to reflect a fixed Z/diparton p_T range of 10 GeV. The target end-to-end signal efficiencies are calculated per bin. The S/\sqrt{B} value is set to 0 wherever target signal efficiency cannot be achieved.

E Performance against $t\bar{t}$ background

The “1-lepton” channel in the $VH(H \rightarrow c\bar{c})$ searches [8, 11] identify $WH(H \rightarrow c\bar{c})$ with the W boson decaying leptonically as the signal process. The major backgrounds in this channel are the $W+jj$ and semileptonic $t\bar{t}$ processes. As far as hadronic reconstruction is concerned, it is expected that the performance of discriminating $WH(H \rightarrow c\bar{c})$ from $W+jj$ events will be similar to the one for discriminating $ZH(H \rightarrow c\bar{c})$ from $Z+jj$ background (cf. Sec. 6). However, since $t\bar{t}$ has a very different signature compared to $Z+jj$, we perform a dedicated study of the performance of the various tagging strategies with $t\bar{t}$ as the background. We use the same simulated $ZH(H \rightarrow c\bar{c})$ signal as a proxy for the $WH(H \rightarrow c\bar{c})$ process to avoid simulating additional processes. This is a valid comparison since only the hadronic parts of the processes are relevant. About 10 million semileptonic $t\bar{t}$ events are simulated following the methods detailed in Sec. 3. Of these, 5 million (*test dataset*) events are used as the background in the following test and the remaining are defined as the *training dataset*.

The same regression and classification models that were trained using $ZH(H \rightarrow b\bar{b})$, $ZH(H \rightarrow c\bar{c})$, and $Z+jj$ samples are used in this study. The respective models are evaluated on AK4, PAIReD, and PAIReDEllipse jets reconstructed in the $t\bar{t}$ sample. Similar to Sec. 6.3.4, event-level BDTs are trained to discriminate $ZH(H \rightarrow c\bar{c})$ events from $t\bar{t}$ events for the three different reconstruction strategies, using the tagger scores, jet kinematics, and Higgs candidate mass (cf. Table 2) as inputs.

The performance of the signal-versus- $t\bar{t}$ event-level BDT is shown in Fig. 19 (left), along with a comparison with the signal-versus- $Z+jj$ BDT (duplicated from Fig. 7 (upper-left)). It can be seen that the discrimination against $t\bar{t}$ is weaker compared to that against $Z+jj$ across all reconstruction scenarios. This can be attributed to the fact that the $t\bar{t}$ event topology is inherently more similar to the signal event topology than the $Z+jj$ topology is, owing to an abundance of heavy-flavor jets in the former. The PAIReDEllipse-based BDT achieves higher maximum signal efficiency compared to the other approaches and achieves a similar gain (factor of ~ 2) in background rejection compared to the AK4 approach at a given signal efficiency. However, the PAIReD approach falls short of the AK4 approach between signal efficiencies of ~ 0.08 to ~ 0.37 , which was not the case for $Z+jj$ background. It can be noted that the classification models used here were trained with only $Z+jj$ as the background for the purpose of demonstrating the strategy.

To perform a fairer comparison, we train extended models of the PAIReD- and PAIReDEllipse-based taggers to incorporate additional classes corresponding to $t\bar{t}$ backgrounds. In addition to the bb , cc , and ll classes in the baseline (3-class) model, we define $bXtt$ and $cXtt$ classes. PAIReD(Ellipse) jets containing at least one b quark from a $t\bar{t}$ event in their area are labelled as $bXtt$. This definition includes non-resonant $b\bar{b}$ pairs in $t\bar{t}$ events. PAIReD(Ellipse) jets containing no b quarks but at least 1 c quark in a $t\bar{t}$ event are labelled $cXtt$. All other PAIReD(Ellipse) jets are labelled ll . New classifier trainings are performed using $ZH(H \rightarrow b\bar{b})$, $ZH(H \rightarrow c\bar{c})$, $Z+jj$, and $t\bar{t}$ samples with 5 classes in the output layer. The $t\bar{t}$ *training dataset* consisting of 5 million semileptonic $t\bar{t}$ events is used for this purpose. The same regression models trained using $ZH(H \rightarrow b\bar{b})$ and $ZH(H \rightarrow c\bar{c})$ samples are used to define the regressed mass of PAIReD(Ellipse) jets.

Once again, two separate event-level BDTs are trained to discriminate $ZH(H \rightarrow c\bar{c})$ events from $Z+jj$ and $t\bar{t}$ backgrounds, respectively, using half of the *test datasets*. The CCvsLL and CCvsBB

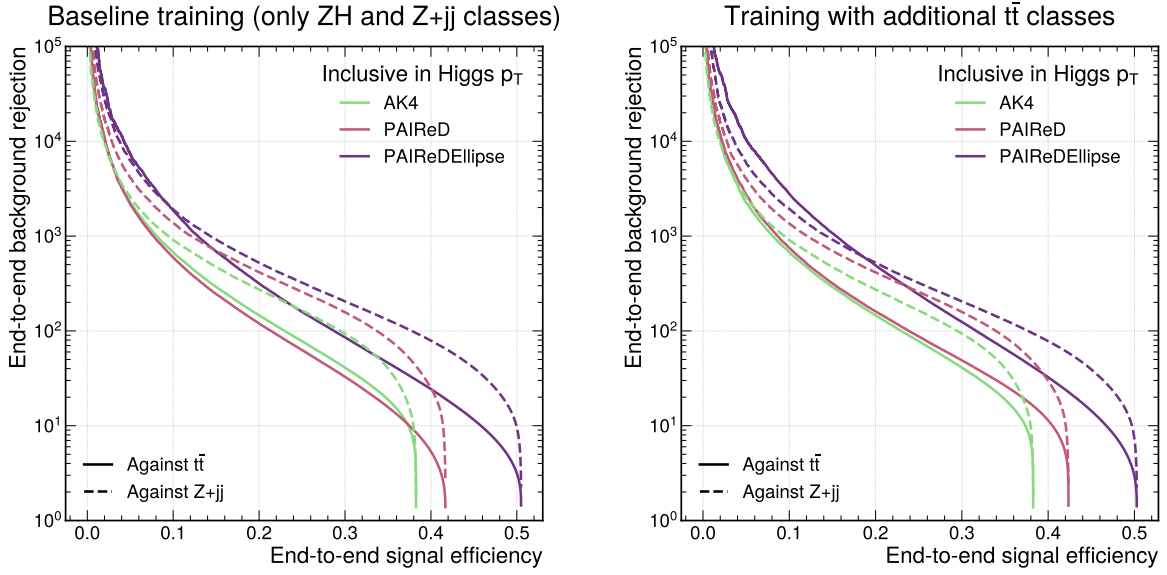


Figure 19: The end-to-end $t\bar{t}$ (the solid lines) and Z+jj (the dashed lines) background event rejection rates as a function of the end-to-end signal efficiency, as predicted by the signal-versus- $t\bar{t}$ and signal-versus-Z+jj event-level BDTs, respectively. The left plot shows the baseline training with only Z+jj samples represented in the trainings, while the right plot shows results of PAIReD(Ellipse) trainings performed with additional $t\bar{t}$ classes. The AK4 trainings are identical in the two plots.

inputs to these BDTs are redefined to include the cX_{tt} and bX_{tt} scores in the denominators, respectively, using predictions from the taggers with extended classes (5-class models). The performances of the retrained signal-versus- $t\bar{t}$ and signal-versus- $Z+jj$ BDTs are evaluated on the remaining half of the *test dataset* and are compared with the results from the baseline AK4-based approach. The comparison is shown in Fig. 19 (right). It can be seen that the PAIReD approach achieves a better performance in rejecting $t\bar{t}$ compared to the AK4 approach when the 5-class model is used. The PAIReDEllipse approach exhibits an even stronger $t\bar{t}$ rejection compared to the corresponding 3-class model. The rejection rates of $Z+jj$ backgrounds are altered only marginally. Therefore, extending the trainings to include jets from various topologies and physics processes appears to improve the generalization capabilities of the taggers. Future studies and experimental implementations may consider including jets from $t\bar{t}$, QCD multijet, and other similar processes as background jets in the training.

F Effects of clustering algorithms

The PAIReD and PAIReDEllipse jets used throughout this paper are constructed without using any sequential clustering algorithms. Their areas are defined using the centers of clustered jets (in this case, AK4 jets) as seeds, and all reconstructed particles lying in the defined area are considered constituents of the jet. This is akin to non-sequential cone algorithms, and in contrast to the commonly-used sequential jet clustering algorithms like the AK and Cambridge-Aachen [71, 72] algorithms in which particles are added to the jet one at a time starting from a seed.

Jet clustering algorithms like AK offer some advantages such as IRC safety [22], and less sensitivity to pileup and unrelated hadronic activities. Infrared safety means that the presence of soft radiation does not affect the results of the algorithm. Collinear safety means that the results of the algorithm remain unaffected after introducing a collinear splitting of one of the inputs. These advantages are lacking when we define PAIReD and PAIReDEllipse jets. On the other hand, previous studies [73–75] have shown that classifiers leveraging IRC-unsafe information outperform classifiers with only IRC-safe inputs in a variety of jet classification tasks. It has been hypothesized that the gain comes from the facts that IRC-unsafe classifiers leverage very-soft radiations from jets, which IRC-safe approaches typically do not have access to, and IRC-unsafe classifiers take exact position of the constituents as inputs, as opposed to IRC-safe approaches taking only relative positions as inputs [75]. The presence of pileup and UE, however, mitigates the gains [73]. In the following subsections, we investigate this phenomenon in the context of PAIReD jets and AK15 jets in the presence of pileup.

F.1 PAIReD jets with AK-clustered particles only

In order to understand the extent of the performance improvement gained by using unclustered particles, we define a new variant of the PAIReD jet approach containing only the reconstructed particles that are clustered inside the seed AK4 jets. This variant, referred to as PAIReDClustered henceforth, does not contain unclustered particles that lie within an angular distance of $\Delta R = 0.4$ around the centers of the seed AK4 jets like PAIReD does, and hence may be considered as an

| | AK4 | PAIReD-Clustered | PAIReD | PAIReD-Ellipse |
|---|----------------|------------------|-----------|----------------|
| Tagging strategy | Individual jet | Jet pairs | Jet pairs | Jet pairs |
| Low-level features of constituents of a thin-radius jet | ✓ | ✓ | ✓ | ✓ |
| Correlations between constituents of two different jets | | ✓ | ✓ | ✓ |
| Soft radiations/unclustered particles around seed jet centers | | | ✓ | ✓ |
| Unclustered particles lying spatially between two seed jets | | | | ✓ |

Table 3: Summary of the information available to the various tagging approaches.

| Signal efficiency | AK4 | PAIReD-Clustered | PAIReD | PAIReD-Ellipse |
|-------------------|-------|------------------|--------|----------------|
| 10 | 908.7 | 1305 | 1373 | 1910 |
| 20 | 273.0 | 394.9 | 415.7 | 523.8 |
| 30 | 93.58 | 143.4 | 157.3 | 205.0 |

Table 4: End-to-end background event rejection rates for different values of end-to-end signal efficiencies (first column) for various algorithms, evaluated with an event-level BDT, inclusively in Higgs boson (or diparton) p_T .

ablated variant of the baseline PAIReD jet defined in this paper. The information available to each tagging strategy is summarized in Table 3.

Dedicated mass regression and classification networks are trained for PAIReDClustered jets with the same samples, labels, and techniques described in Secs. 3–5. An event level BDT to discriminate $ZH(H \rightarrow c\bar{c})$ signal events from $Z+jj$ backgrounds is trained following the prescription discussed in Sec. 6.3.4 and using the same input variables corresponding to the PAIReD jet column in Table 2. The end-to-end background event rejection rate is plotted as a function of the end-to-end signal efficiency for the AK4 approach and the three variants of the PAIReD approach, as is shown in Fig. 20. The rates are also summarized in Table 4 for three different signal efficiencies.

It can be seen that the performance of the PAIReDClustered tagging approach is marginally worse than that of the PAIReD approach, but significantly better than that of the AK4 approach. On the one hand, this shows that the improvement in the PAIReD approach over traditional algorithms arises almost exclusively from leveraging correlations between low-level features of two different

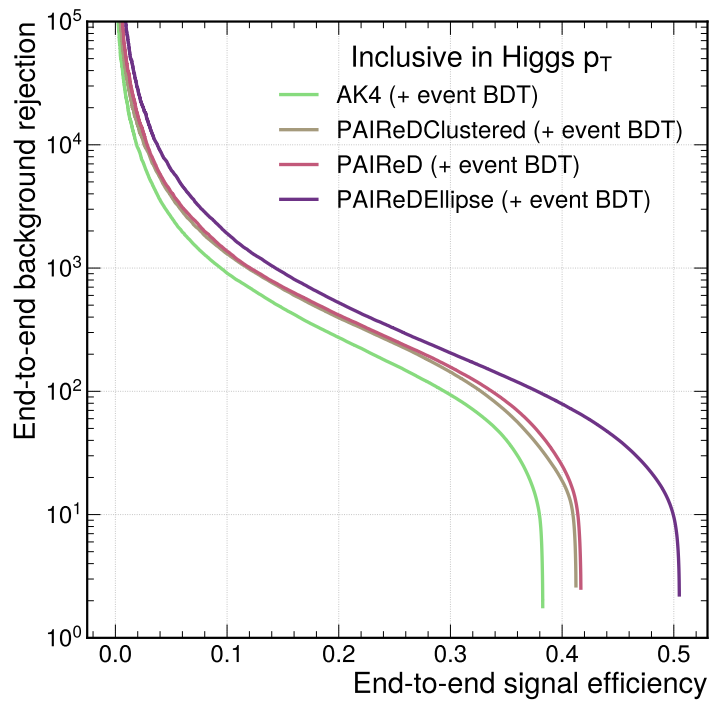


Figure 20: The end-to-end background event rejection rate as a function of the end-to-end signal efficiency inclusively in Higgs boson (or diparton) p_T as predicted by event-level BDTs.

jets arising from the same heavy particle. An additional, small improvement is gained from using soft, unclustered particles around the seed jet centers; this observation is in agreement with those in Refs. [73–75]. On the other hand, this also shows that it is possible to use an alternative, ablated variant of the PAIReD approach and still improve over traditional approaches, in case the PS, UE, and pileup—and hence the unclustered particles used by the baseline PAIReD variant—cannot be modeled correctly in simulations.

F.2 AK15 and Cone15 jets

To examine the effect of unclustered particles in tagging large-radius jets, we additionally define a cone-based jet (Cone15) with radius 1.5 units, for every AK15 jet reconstructed in the simulated events. The axis of every Cone15 jet is defined to be at the center of the corresponding AK15 jet and all particles in a radius of $\Delta R = 1.5$ units around the jet axis are considered its constituents. This makes the Cone15 jets geometrically similar to the AK15 jets with the difference that the former does not use the AK algorithm, except for defining the jet center. The regression and classification trainings (Sec. 5) and the mock $ZH(H \rightarrow c\bar{c})$ analysis (Sec. 6) are repeated replacing AK15 jets with Cone15 jets.

The maximum signal efficiencies, classifier AUCs, end-to-end background rejections, and signal sensitivity estimates in the context of a $ZH(H \rightarrow c\bar{c})$ analysis are shown in Fig. 21. The Cone15 and AK15 have similar signal reconstruction efficiencies, except for at high Higgs boson boosts where the Cone15 approach reconstructs about 2% more signal events. The Cone15 approach selects the correct jet as the Higgs boson candidate in a slightly higher number of events, resulting in this observed gain in signal reconstruction efficiency. However, this gain is offset by the classifier performance in the next step, where the AK15-based classifier performs better only at high boosts ($p_T \gtrsim 350$ GeV) of the Higgs boson. The Cone15-based classifier has a significantly better classification performance at lower boosts. The combined effect can be seen in the end-to-end background rejection and signal sensitivity plots, where the two approaches show similar performances, with the Cone15 performing marginally better at low boosts ($\lesssim 300$ GeV), while the AK15-based approach performs better at higher Higgs boson p_T 's ($\gtrsim 350$ GeV).

The improvement in the classification performance at low Higgs boson boosts using the Cone15 approach suggests that the presence of particles (mostly soft radiations) in addition to the ones clustered by the AK algorithm within the jet radius helps improve the classifier's accuracy at higher angular separation of the partons. However, the difference in the final end-to-end background rejection is marginal, as few AK15 jets are reconstructed at low boosts. On the other hand, a similar performance between the two approaches at higher boosts suggests that a sequential clustering algorithm may be more crucial at low angular separation of the partons, where the hadronization products of the two partons have a larger overlap.

The study in this subsection is limited to only one example and the conclusions drawn here are empirical. A detailed description and a theoretical analysis of the synergistic effects of various jet clustering methods and attention-based deep learning networks are beyond the scope of this paper. Nevertheless, the performance of the PAIReDEllipse strategy may potentially be improved at high boosts in the future by utilizing advanced jet grooming and pileup mitigation techniques [76–80], and potentially at all boosts by replacing the AK4 seeds with jets constructed with newer

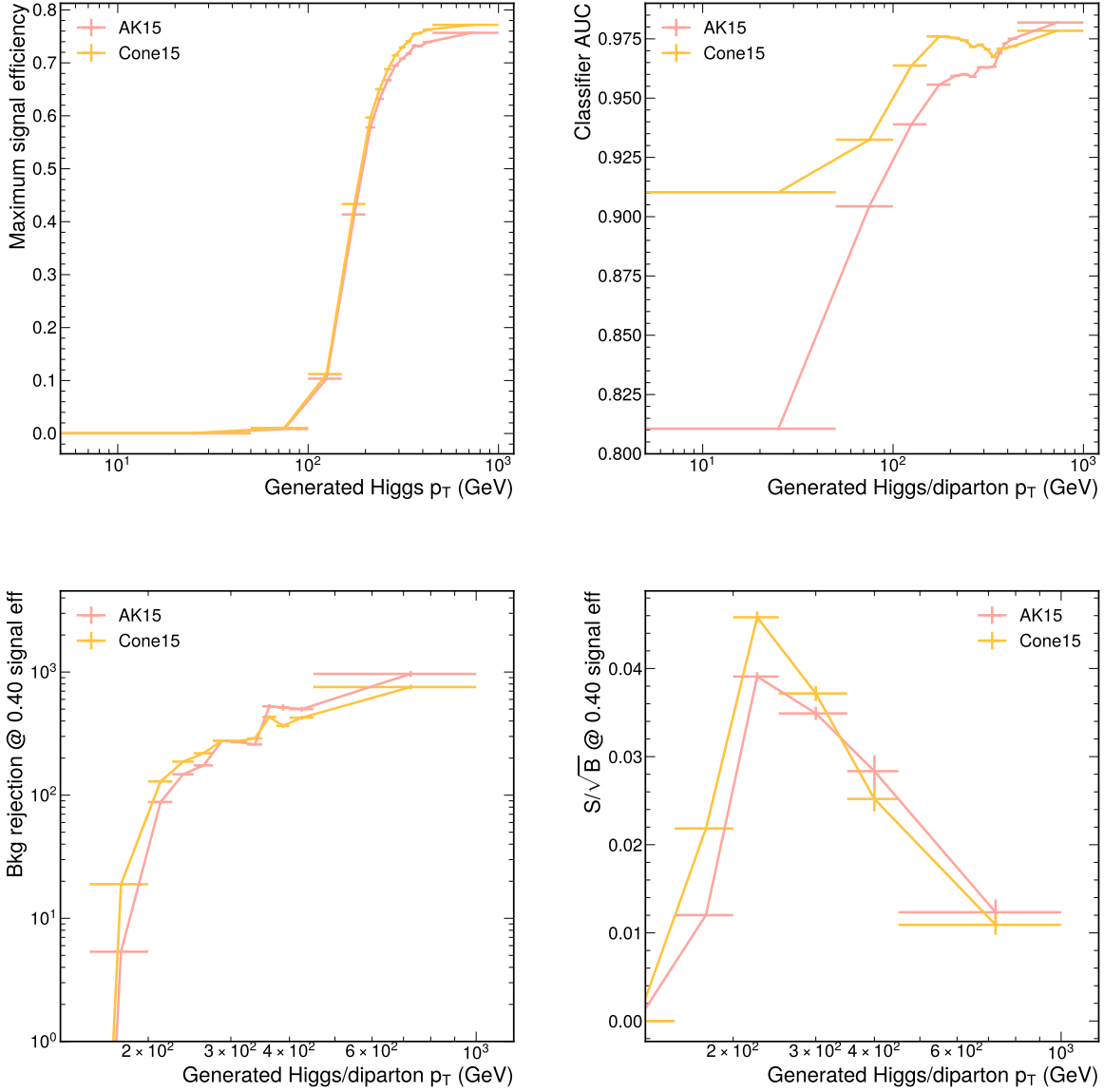


Figure 21: The maximum signal efficiency (upper-left), the classifier AUCs (upper-right), and the end-to-end background rejection rate (lower-left) and signal sensitivity (lower-right) at an end-to-end signal efficiency of 0.4 are plotted as a function of Higgs boson p_T (or diparton p_T) comparing the AK15- and Cone15-based approaches.

algorithms, such as XCone [81, 82], dynamic-radius algorithms [83, 84], SIFT [85], or supervised jet clustering [86]. These comparisons could be investigated in future studies.